# Chemical Engineering Journal

## Bi0.5Sb1.5Te3/PEDOT:PSS-Based Flexible Thermoelectric Film and Device

--Manuscript Draft--

| | |
|---|---|
| **Manuscript Number:** | CEJ-D-20-02765R1 |
| **Article Type:** | Research Paper |
| **Keywords:** | Thermoelectrics; Flexible; PEDOT:PSS; Bismuth telluride; Interface |
| **Corresponding Author:** | Zhi-Gang Chen, Ph.D.<br>University of Southern Queensland<br>Brisbane, AUSTRALIA |
| **First Author:** | Yuan Wang |
| **Order of Authors:** | Yuan Wang |
| | Min Hong |
| | Weidi Liu |
| | Xiao-Lei Shi |
| | Sheng-Duo Xu |
| | Qiang Sun |
| | Han Gao |
| | Siyu Lu |
| | Jin Zou |
| | Zhi-Gang Chen, Ph.D. |
| **Abstract:** | Incorporating inorganic thermoelectric fillers into conductive polymers is one promising strategy to develop high-performance flexible thermoelectric films. However, due to the relatively high interfacial contact resistance between fillers and polymers, carriers tend to be scattered at the interfaces during the interfacial transports, which deteriorates the electrical properties of the system, and in turn leads to low energy conversion efficiency. Here, a new strategy is developed to optimize interfacial carrier transports in Bi0.5Sb1.5Te3/PEDOT:PSS composite, by coating Bi0.5Sb1.5Te3 fillers with highly conductive CuTe layer. With highly crystallized PEDOT:PSS prepared as the matrix, high-performance Cu-Bi0.5Sb1.5Te3 /PEDOT:PSS film is fabricated with promising σ of ~2300 S cm-1 and peak S2σ of 312 μW m-1 K-2 at room temperature, which reaches to a record-high value in the reported Bi0.5Sb1.5Te3/PEDOT:PSS composites. Accordingly, a home-made flexible thermoelectric device is fabricated using our prepared composites, generating a promising open-circuit thermovoltage of ~7.7 mV with the human wrist as the thermal source. This study addresses the significance of interfacial carrier transport, hinting the bright prospects of cheap conductive polymers as the effective power source of wearable electronics. |
| **Response to Reviewers:** | Response to Editor and Reviewers<br>Response to Editor<br>General comment: suggested title: "Flexible Thermoelectric Film and Device based on Bi0.5Sb1.5Te3/PEDOT:PSS".<br>Response: We appreciate the Editor's valuable suggestion. We have modified the title as "Bi0.5Sb1.5Te3/PEDOT:PSS-Based Flexible Thermoelectric Film and Device".<br><br>Response to Reviewer 1<br>General comment: Reviewer #1: In this manuscript, the authors paid their works on the surface engineering of BST/PEDOT:PSS composite material to develop a promising thermoelectric materials. This developed material can be presented a as large as power factor of 312 μW m-1 K-2 due to the highly conductive CuTe layer. Before be published in Chemical Engineering Journal, few questions should be solved.<br><br>Comment 1: Please check the spell of reductionr in Fig. 5b.<br>Response: We appreciate the positive comments from the reviewer. We have |

corrected the spell in Fig. 5b.

Comment 2: To illustrate the flexibility of the BST/PEDOT:PSS thermoelectric material, the authors should evaluate the thermoelectric performance of BST/PEDOT:PSS under stretching or bending conditions.
Response: The bending experiment of the as-fabricated BST/PEDOT:PSS thermoelectric films is shown in the photos of Fig. 1 and home-made flexible device of Fig. 6b. Their thermoelectric performances under stretching or bending conditions have also been tested by attaching home-made flexible thermoelectric device onto human wrist and chest, followed by measuring generated thermovoltages, as illustrated in Fig. 6c.

Moreover, in regards to measurements of free-standing films in bending conditions, since we employed SBA458 (Netzsch) to evaluate the film electrical properties, the film sample is required to be loaded on the top of thermocouples and current pins, as shown in Fig. R1, with polytetrafluoroethylene (PTFE) cover pressing on the top to fix samples during the measurement and ensure decent contacts between samples and pins. After stretching or bending the as-fabricated BST/PEDOT:PSS thermoelectric films for several times, we used the same way to measure their thermoelectric properties. Similar results can be obtained.

Fig. R1. Schematic illustration of SBA458 working mechanism and photos of laboratory equipment. (a) Schematic of working mechanism in SBA 458. (b) Non-loaded SBA 458 in the laboratory. (c) Loaded SBA 458 in the laboratory.

Comment 3: Combining inorganic materials with high thermoelectric properties and flexible conductive materials is a feasible strategy to develop flexible thermoelectric materials, a good case of Chem. Eng. J. 320 (2017) 201-210 should be referred.
Response: We have cited the mentioned article as the reference [51] of the revised manuscript.”

Response to Reviewer #3
General comment: In this manuscript, the authors prepared an PEDOT:PSS/inorganic hybrid material with excellent thermoelectric performance originating from so-called interfacial engineering. This conception is intriguing. However, the discussion is weak and incomplete, especially for the variation of Seebeck coefficient of the hybrid materials. Furthermore, the carrier transportation between interfaces is barely discussed, not to mention the optimization process. The relation between material design and thermoelectric performance is not well established. I didn't recommend this current work to be published in Chemical Engineering Journal until a completion of a number of appropriate amendments according to the following points.

Comment 1: What's the basic principle to optimize the carrier transportation in the interfacial region between organic and inorganic materials? If introducing a more conductive coating or element is fine, why copper is selected instead of other noble elements?
Response: We appreciate the constructive comments from the reviewer. The basic principle to optimize interfacial carriers transport between organic and inorganic materials lies in the reduction of interfacial contact resistance to prevent intense interfacial carrier scatterings.[1-3] Cu coating towards BST fillers is initially designed based on below two reasons. Firstly, Cu exhibits outstanding electrical conductivity, which holds great promises to reduce the interfacial contact resistance and carrier scatterings. Secondly, Cu coating towards BST thermoelectric materials has been confirmed to result in the significant boost of electrical properties by our previous works.[4, 5] Considering this, Cu-BST fillers are promising to have increased hybrid thermoelectric performances than single BST fillers. Other coatings using noble metals such as Ag and Ni are also promising and deserve our future studies.

Comment 2: In this case there is a CuTe phase between PEDOT:PSS and BST according to the HRTEM and XRD results, i.e., two interfacial region may exist in this hybrid system: one laid between PEDOT crystalline and CuTe, and another laid between CuTe and BST. Structure characterization is well presented. But the carrier transport between these interfaces is barely discussed. A more solid experimental evidence or mathematical model should be provided to quantitatively illustrate that the

carrier transportation between these interfaces has been optimized.
Response: As-claimed optimization of interfacial carrier transports mainly occurs between polymers and fillers, which is at the interface between BST and PEDOT before Cu coatings, and CuTe and PEDOT after Cu coatings. It is not critical to consider the interface between CuTe and BST, as our study utilized chemical coating and Cu-BST as the filler is considered as a whole, whose thermoelectric performances are suggested in Fig. S1 in the Supporting Information.

In order to manifest the optimization of interfacial carrier transports between polymers and fillers. Experimentally, boosted system electrical conductivity in Fig. 4a and increased carrier mobilities in Table 1 are observed. Theoretically, we also calculate series- and parallel-connection models of hybrid films and compare with our experimental results, which are added to the Supporting Information. Specifically, parallel- and series-connection model are given as[6, 7]

$$\sigma_{parallel}=\sigma_{PEDOT}(1-x)+\sigma_{filler}x, \quad (1)$$

$$S_{parallel}=((1-x)\sigma_{PEDOT}S_{PEDOT}+x\sigma_{filler}S_{filler})/((1-x)\sigma_{PEDOT}+x\sigma_{filler}), \quad (2)$$

$$\sigma_{series}=(\sigma_{filler}\sigma_{PEDOT})/(\sigma_{filler}(1-x)+\sigma_{PEDOT}x), \text{ and} \quad (3)$$

$$S_{series}=(S_{filler}\kappa_{PEDOT}x+S_{PEDOT}\kappa_{filler}(1-x))/(\kappa_{PEDOT}x+\kappa_{filler}(1-x)), \quad (4)$$

where x is the volume fraction of fillers. We compare the calculation results with experimental results with 4wt. % filler content, and the results are shown in Fig. R2 (Fig. S3 in the Supporting Information).

Fig. R2. Experimental (a) electrical conductivity and (b) Seebeck coefficient of 4wt. % filler content hybrid film compared with calculation results of series- and parallel-models.

Without Cu coating, both the electrical conductivity and Seebeck coefficient lie beyond the prediction range. This can be understood as that most carriers are scattered at the interface, deteriorating system electrical properties. After Cu coating, the system shows reasonable results within the prediction range, which indicates the “blocking” effects of fillers are mitigated due to reduced interfacial contact resistance. This contrast supports our claim of optimized interfacial transport.

Relevant discussions have been added to Page 14 of the revised manuscript as “To manifest above claims, series- and parallel-connection models are employed to predict σ and S of hybrid films with 4wt. % filler content and compare with our experimental results. The results are illustrated in Fig. S3. Without Cu coating, both σ and S lie beyond the prediction range. This can be understood as that most carriers are scattered at the interface, deteriorating system electrical properties. After Cu coating, the system shows reasonable results within the prediction range, which indicates the “blocking” effects of fillers are mitigated due to reduced interfacial contact resistance. This contrast supports our claims of optimized interfacial transport.”

Comment 3: Table 1 presented that the mobility and concentration of carrier of hybrid materials simultaneously increased with the introduction of Cu. Yet based on the Boltzmann transportation theory model, the Seebeck coefficient has a negative correlation with the
carrier concentration. Meanwhile, the Seebeck coefficient of hybrid material with 4 wt% filler firstly increased and then dropped with the introduction of Cu. Authors should give a further explanation on this variation and clarify what kind of role did CuTe layer play in this variation.
Response: The increase of carrier concentration is caused by Cu introduction into the hybrid system. This is underpinned by Fig. S1c, where significantly boosted carrier concentrations are observed after Cu coatings. The enhancement of system carrier mobility, on the other hand, stems from reduced interfacial contact resistance induced by CuTe layer, where less carriers are scattered during the interfacial transports.

Relevant discussions have been added on Page 16 of the revised manuscript as “Hall measurements are applied to investigate the change of system carrier concentration (n) and μ before and after Cu coatings, and Table 1 summarizes the results. n is observed to improve from ~8.06 to ~8.28 and ~8.37 × 1020 cm-3 after Cu coatings,

which is caused by the introduction of Cu, as manifested by n of BST before and after Cu coatings in Figure S1c. Effective increased μ occurs from ~13.72 to ~18.04 and ~18.82 cm2 V-1 s-1 after Cu coatings. This verifies the optimization of interfacial carrier transports and accounts for increased σ."

The negative relationship between carrier concentration and Seebeck coefficient depicted by Boltzmann transportation theory model follows Pisarenko relation:[8]
$S=(8\pi^2 k_B^2)/(3eh^2 ) m^* T 〖(\pi/3n)〗^(2/3),$ (5)
where kB, h and m* are the Boltzmann constant, the Planck constant, and the density of states (DOS) effective mass, respectively. However, such a relationship is proposed based on the assumption that carriers are delocalized.[9] These are inconsistent with carrier transports and structures of conductive polymers.[10] Specifically, conductive polymers can be structurally considered as highly conductive crystalline domains surrounded by poorly conductive amorphous matrices.[11, 12] Crystalline domains within conductive polymers possess ordered stackings of rigid conjugated chains from π-π interactions, leading to the relatively unimpeded transport of electrons,[13-15] while amorphous domains exhibit localized electrons transport, due to significantly dampened carrier mobility from amorphous chain stacking.[13] Therefore, Pisarenko relation is not thoroughly applicable for conductive polymers.

Actually, the variation of Seebeck coefficient in our study can be explained by the interfacial energy filtering effect between polymer matrix and inorganic fillers.[16-19] Specifically, carriers tend to be severely scattered at the interface without CuTe layer (no interfacial energy filtering), while passing through fillers with CuTe layer due to reduced interfacial contact resistance, inducing the interfacial energy filtering. This explains the increase of Seebeck coefficient after Cu coating. With increasing the amount of Cu coating, Cu-BST filler presents reduced Seebeck coefficient due to increased carrier concentration, as shown in Fig. S1b and c in the Supporting Information, leading to slightly dropped system Seebeck coefficient.

Relevant discussion has been modified on Page 16 of the revised manuscript as "On the other hand, it should be noted that Cu-BST fillers (both 0.05 wt.% and 0.1 wt.%) possess more obvious boost towards S compared with BST fillers. This may because introduced CuTe layers reduce interfacial contact resistance, allowing more carriers to transport through BST fillers to induce more sufficient interfacial energy filtering. With the increasing amount of Cu coating, S of Cu-BST fillers reduces due to increased n, as show in Figure S1b and c, which consequently leads to slightly dropped system S."

Comment 4: There is poor discussion on the band diagram in Figure 4b. How did the authors get the band structure basically involving LOMO, HOMO and EF of the hybrid materials or individual components? What's the meaning of this diagram? Did this relate to interfacial-engineering? Why a high average energy is favorable to a high Seebeck coefficient?
Response: The band structure of hybrid is schematically plotted based on work functions and Fermi levels locations of each individual component. Specifically, in the hybrid system, system Fermi level is firstly assumed at one energy level.[16-18] Then the positions of LOMO and HOMO for polymers or CB and VB for inorganic fillers are plotted based on their relative positions to their own Fermi levels. Finally, based on the energy offset between filler VB and polymer HOMO, the interfacial energy barrier is determined.

The meaning of this plot is to schematically illustrate the interfacial energy filtering process occurred at the interfaces, which accounts for the increase of system Seebeck coefficient. Interfacial energy filtering of carriers as one important process at the interface is related to interfacial engineering.

The relationship between Seebeck coefficient and carrier energy can be explained in the below way. For degenerately doped thermoelectric materials, Seebeck coefficient as a function of the energy dependence of the electrical conductivity follows Mott relation[20]
$S=\pi^2/3 〖(k_B^2 T)/e \{d[\ln(\sigma(E))]/dE\}_(E=E_(I^' ) )〗^ ,$
(6)
where kB is the Boltzmann constant. Meanwhile, taken at the Fermi energy for degenerate semiconductors, or at any value of E and integrated over energy in the

general case, electrical conductivity can be described as
$\sigma = ne\mu = (ne^2 \tau)/m^*$ , (7)
where $m^*$ is the effective mass and $\tau$ is the relaxation time, which can be further described as
$\tau = \tau_0 E^{(\lambda - 1/2)}$, (8)
where $\lambda$ is the scattering parameter, typically $\lambda = 0$ for scattering of electrons by acoustic phonons, and $\lambda = 2$ for scattering of electrons by ionized impurities.[21] The trend can be found that with higher carrier energy E obtained, $\tau$ can be boosted, leading to higher $\sigma$ and accordingly higher S.[22]

Comment 5: According to XRD results in Figure 3(a), PEDOT crystalline occurred after pre- and post-treatment. Yet in Figure 3(d), authors insisted that the fringe pattern is inorganic filler. Why it can't be the PEDOT crystalline?
Response: The ordering effect towards conductive polymers by pre- and post-treatments leads to lamella stacking in the microstructure (enhanced crystallinity). However, as can be seen from the cross-sectional SEM images in Fig. 3b, the distance between stackings should be tens of nanometre, while the d-spacing in Fig. 3d is less than 1 nm. Therefore, the fringe pattern should reflect inorganic filler rather than PEDOT crystalline.

Response to Reviewer #4
General comment: In this study, the authors reported a new methodology to optimize the interfacial carriers transport in $Bi_{0.5}Sb_{1.5}Te_3$/PEDOT:PSS composite, by coating $Bi_{0.5}Sb_{1.5}Te_3$ fillers with highly conductive CuTe layer. Due to synergistic improvements of electrical conductivity and Seebeck coefficient, a promising electrical conductivity of ~2300 S cm-1 and impressive power factor of 312 μW m-1 K-2 have been achieved at room temperature. Moreover, a home-made flexible thermoelectric device has been fabricated to generate a open-circuit thermovoltage of ~7.7 mV with the human wrist as the thermal source.
Basically, this work is a comprehensive study with systematic analysis and discussions. The observed boosted interfacial carriers transport and record power factor of 312 μW m-1K-2 might be of great interest to researchers of inorganic/organic flexible thermoelectric field. Additionally, as-fabricated flexible thermoelectric generator shows full potentials to generate electricity with human body, which could be novel for thermoelectric clothes developments. Therefore, I suggest to accept this paper for publication after the consideration of the following minor issues:

Comment 1: In terms of $Bi_{0.5}Sb_{1.5}Te_3$ filler size, the inset BSE image of Figure 2b shows the size of several hundreds of nanometres. However, the TEM image of 6 wt.% Cu-BST/PEDOT:PSS film in Figure 3d indicates filler size less than 100 nm. How would you explain this?
Response: We appreciate the positive comments from the reviewer. The smaller $Bi_{0.5}Sb_{1.5}Te_3$ filler size observed in Fig. 3d than Fig. 2b can be attributed to blocking effects of conductive polymers towards TEM electron beams, where partial lattice structures of inorganic fillers underneath conductive polymers cannot be observed.

One typical SEM image of as-prepared $Bi_{0.5}Sb_{1.5}Te_3$ fillers is provided in Fig. R3 (Fig. S2 in the Supporting Information). It can be found filler size is ~400 nm, which is consistent with Fig. 2b.

Fig. R3. Typical SEM images of as-prepared $Bi_{0.5}Sb_{1.5}Te_3$ fillers.

Relative discussions have been added to Page 13 of the revised manuscript as “It should be noted that the size of fillers in our study are typically ~400 nm, as shown in Fig. S2. The smaller filler size observed in Fig. 3d can be attributed to blocking effects of conductive polymers towards TEM electron beams, where partial lattice structures of inorganic fillers underneath conductive polymers cannot be observed.”

Comment 2: As described by the experimental section, conductive polymer PEDOT:PSS was treated sequentially by pre- and post-treatments to increase the crystallinity. During the post-treatments, PEDOT:PSS needs to be fabricated into films in order to be immersed into concentrated $H_2SO_4$. In this case, how can PEDOT:PSS be incorporated with fillers later to prepare the TE ink?
Response: PEDOT:PSS films after DMSO pre-treatment and concentrated $H_2SO_4$

post-treatment are transformed into PEDOT:PSS slurry by intensively stirring films overnight on the magnetic stir plate. The uniform TE ink is then prepared by thoroughly mixing PEDOT:PSS slurry with Bi0.5Sb1.5Te3 fillers. Relevant discussions can be found in Experimental Section as “The as-treated PEDOT:PSS films were lastly magnetically stirred into PEDOT:PSS slurry, which was ready for the film fabrication.”

Comment 3: The authors ascribed the improvements of Seebeck coefficient to interfacial energy filtering effects, which is reasonable. However, only filtering effects between BST and PEDOT:PSS are considered. Why the effects of as-coated highly conductive CuTe layer are neglected?
Response: The interfacial energy filtering effect of CuTe is neglected in our study considering the following two reasons. Firstly, as manifested by high-magnitude TEM images of BST fillers in Fig. 2, as-coated CuTe layer is only ~17 nm, whose tiny amount can be neglected compared with ~400 nm BST fillers. Secondly, CuTe presents alloy-like electrical properties with the Fermi level deeply lying in the valance band, whose capacity to filter holes during the transport is quite rare, which can be ignored.

Reference

[1] B. Zhang, J. Sun, H.E. Katz, F. Fang, R.L. Opila, Promising Thermoelectric Properties of Commercial PEDOT:PSS Materials and Their Bi2Te3 Powder Composites, ACS Applied Materials & Interfaces 2 (2010) 3170-3178.
[2] X.B. Zhao, S.H. Hu, M.J. Zhao, T.J. Zhu, Thermoelectric properties of Bi0.5Sb1.5Te3/polyaniline hybrids prepared by mechanical blending, Materials Letters 52 (2002) 147-149.
[3] N. Toshima, N. Jiravanichanun, H. Marutani, Organic Thermoelectric Materials Composed of Conducting Polymers and Metal Nanoparticles, Journal of Electronic Materials 41 (2012) 1735-1742.
[4] Z. Huang, H. Zhang, K. Zheng, X. Dai, Y. Yu, H. Cheng, F. Zu, Z.-G. Chen, Enhancing thermoelectric performance of Cu-modified Bi0.5Sb1.5Te3 by electroless plating and annealing, Progress in Natural Science: Materials International 28 (2018) 218-224.
[5] Z. Huang, X. Dai, Y. Yu, C. Zhou, F. Zu, Enhanced thermoelectric properties of p-type Bi 0.5 Sb 1.5 Te 3 bulk alloys by electroless plating with Cu and annealing, Scripta Materialia 118 (2016) 19-23.
[6] L. Wang, Z. Zhang, Y. Liu, B. Wang, L. Fang, J. Qiu, K. Zhang, S. Wang, Exceptional thermoelectric properties of flexible organic−inorganic hybrids with monodispersed and periodic nanophase, Nature Communications 9 (2018) 3817.
[7] H. Ju, J. Kim, Chemically Exfoliated SnSe Nanosheets and Their SnSe/Poly(3,4-ethylenedioxythiophene):Poly(styrenesulfonate) Composite Films for Polymer Based Thermoelectric Applications, ACS Nano 10 (2016) 5730-5739.
[8] R. Moshwan, L. Yang, J. Zou, Z.-G. Chen, Eco-Friendly SnTe Thermoelectric Materials: Progress and Future Challenges, 27 (2017) 1703278.
[9] J. Zhou, X. Li, G. Chen, R. Yang, Semiclassical model for thermoelectric transport in nanocomposites, Physical Review B 82 (2010) 115308.
[10] S.D. Kang, G.J. Snyder, Charge-transport model for conducting polymers, Nature Materials 16 (2017) 252-257.
[11] A.J. Epstein, J.M. Ginder, F. Zuo, H.S. Woo, D.B. Tanner, A.F. Richter, M. Angelopoulos, W.S. Huang, A.G. MacDiarmid, Insulator-to-Metal Transition in Polyaniline Effect of Protonation in Emeraldine, Synthetic Met 21 (1987) 63-70.
[12] P. Sheng, J. Klafter, Hopping Conductivity in Granular Disordered Systems, Phys Rev B 27 (1983) 2583-2586.
[13] O. Bubnova, X. Crispin, Towards Polymer-Based OrganicThermoelectric Generators, Energy Environ. Sci. 5 (2012) 9345.
[14] P.J. Brown, D.S. Thomas, A. Köhler, J.S. Wilson, J.-S. Kim, C.M. Ramsdale, H. Sirringhaus, R.H. Friend, Effect of Interchain Interactions on the Absorption and Emission of Poly(3-hexylthiophene), Phys Rev B 67 (2003) 064203.
[15] C.A. Hunter, J.K.M. Sanders, The Nature of π-π Interactions, J Am Chem Soc 112 (1990) 5525-5534.
[16] M. He, J. Ge, Z. Lin, X. Feng, X. Wang, H. Lu, Y. Yang, F. Qiu, Thermopower enhancement in conducting polymer nanocomposites via carrier energy scattering at the organic–inorganic semiconductor interface, Energy & Environmental Science 5 (2012) 8351.

[17] C. Gayner, Y. Amouyal, Energy Filtering of Charge Carriers: Current Trends, Challenges, and Prospects for Thermoelectric Materials, Advanced Functional Materials (2019) 1901789.
[18] J. Choi, J.Y. Lee, S.-S. Lee, C.R. Park, H. Kim, High-Performance Thermoelectric Paper Based on Double Carrier-Filtering Processes at Nanowire Heterojunctions, Advanced Energy Materials 6 (2016) 1502181.
[19] Z. Liang, M.J. Boland, K. Butrouna, D.R. Strachan, K.R. Graham, Increased power factors of organic–inorganic nanocomposite thermoelectric materials and the role of energy filtering, Journal of Materials Chemistry A 5 (2017) 15891-15900.
[20] N.F. Mott, E.A. Davis, Electronic Processes in Non-crystalline Materials, Oxford, Clarendon, 1979.
[21] J.P. Heremans, C.M. Thrush, D.T. Morelli, Thermopower enhancement in PbTe with Pb precipitates, Journal of Applied Physics 98 (2005) 063703.
[22] J.P. Heremans, C.M. Thrush, D.T. Morelli, Thermopower enhancement in lead telluride nanostructures, Physical Review B 70 (2004) 115334.

THE UNIVERSITY OF QUEENSLAND
AUSTRALIA

**Materials Engineering**
**School of Mechanical and Mining Engineering**

**HONNARARY ASSOCIATE PROFESSOR**
Zhi-Gang Chen, BEn, PhD

The University of Queensland
Brisbane QLD 4072 Australia
Telephone (07) 3346 3195
International +61-7-33654183
Facsimile (07) 3346 3993
Email zhigang.chen@uq.edu.au
URL: http://researchers.uq.edu.au/researcher/1676
CRCOS PROVIDER NUMBER 00025B

Dear Editor,

With this letter, I am pleased to resubmit our revised manuscript entitled "**$Bi_{0.5}Sb_{1.5}Te_3$/PEDOT:PSS-based Flexible Thermoelectric Film and Device**" for your consideration as a full paper published in **Chemical Engineering Journal.** I certify that this is an original manuscript that is not submitted elsewhere for publication.

We sincerely appreciate your and reviewers' comments on our earlier submission. We have addressed all the comments from you and reviewers in the revised manuscript. We believe our work would appeal to broad audience in the field of thermoelectric materials, as well as wider communities of functional materials, physics science, and chemistry, so that this research article is deserved be accepted for a publication in your prestigious journal.

Look forward to hearing from you.

Sincerely yours,

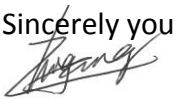

Zhi-Gang CHEN

# Suggested Reviewers

**Lidong Zhao**

Professor, Beihang University

zhaolidong@buaa.edu.cn

Expert in developing thermoelectric materials

**Tiejun Zhu**

Professor, Zhejiang University

zhutj@zju.edu.cn

Expert in thermoelectric materials

**Xiaolin Wang**

Professor, University of Wollongong

xiaolin@uow.edu.au

Expert in understanding mechanisms of enhancing thermoelectric performance

**Kanishka Biswas**

Associate Professor, Jawaharlal Nehru Centre for Advanced Scientific Research

kanishka@jncasr.ac.in

Expert in characterization and mechanism-understanding of thermoelectric materials

**Jiaqing He**

Professor, Southern University of Science and Technology

hejq@sustech.edu.cn

Expert in thermoelectric materials characterization and analysis

# Response to Editor and Reviewers

## Response to Editor

***General comment:*** *suggested title: "Flexible Thermoelectric Film and Device based on Bi0.5Sb1.5Te3/PEDOT:PSS".*

**Response:** We appreciate the Editor's valuable suggestion. We have modified the title as "$Bi_{0.5}Sb_{1.5}Te_3$/PEDOT:PSS-Based Flexible Thermoelectric Film and Device".

**Response to Reviewer 1**

***General comment:*** *Reviewer #1: In this manuscript, the authors paid their works on the surface engineering of BST/PEDOT:PSS composite material to develop a promising thermoelectric materials. This developed material can be presented a as large as power factor of 312 μW $m^{-1}$ $K^{-2}$ due to the highly conductive CuTe layer. Before be published in Chemical Engineering Journal, few questions should be solved.*

***Comment 1:*** *Please check the spell of reductionr in Fig. 5b.*

**Response:** We appreciate the positive comments from the reviewer. We have corrected the spell in **Fig. 5b**.

***Comment 2:*** *To illustrate the flexibility of the BST/PEDOT:PSS thermoelectric material, the authors should evaluate the thermoelectric performance of BST/PEDOT:PSS under stretching or bending conditions.*

**Response:** The bending experiment of the as-fabricated BST/PEDOT:PSS thermoelectric films is shown in the photos of **Fig. 1** and home-made flexible device of **Fig. 6b**. Their thermoelectric performances under stretching or bending conditions have also been tested by attaching home-made flexible thermoelectric device onto human wrist and chest, followed by measuring generated thermovoltages, as illustrated in **Fig. 6c**.

Moreover, in regards to measurements of free-standing films in bending conditions, since we employed SBA458 (Netzsch) to evaluate the film electrical properties, the film sample is required to be loaded on the top of thermocouples and current pins, as shown in **Fig. R1**, with polytetrafluoroethylene (PTFE) cover pressing on the top to fix samples during the measurement and ensure decent contacts between samples and pins. After stretching or bending

the as-fabricated BST/PEDOT:PSS thermoelectric films for several times, we used the same way to measure their thermoelectric properties. Similar results can be obtained.

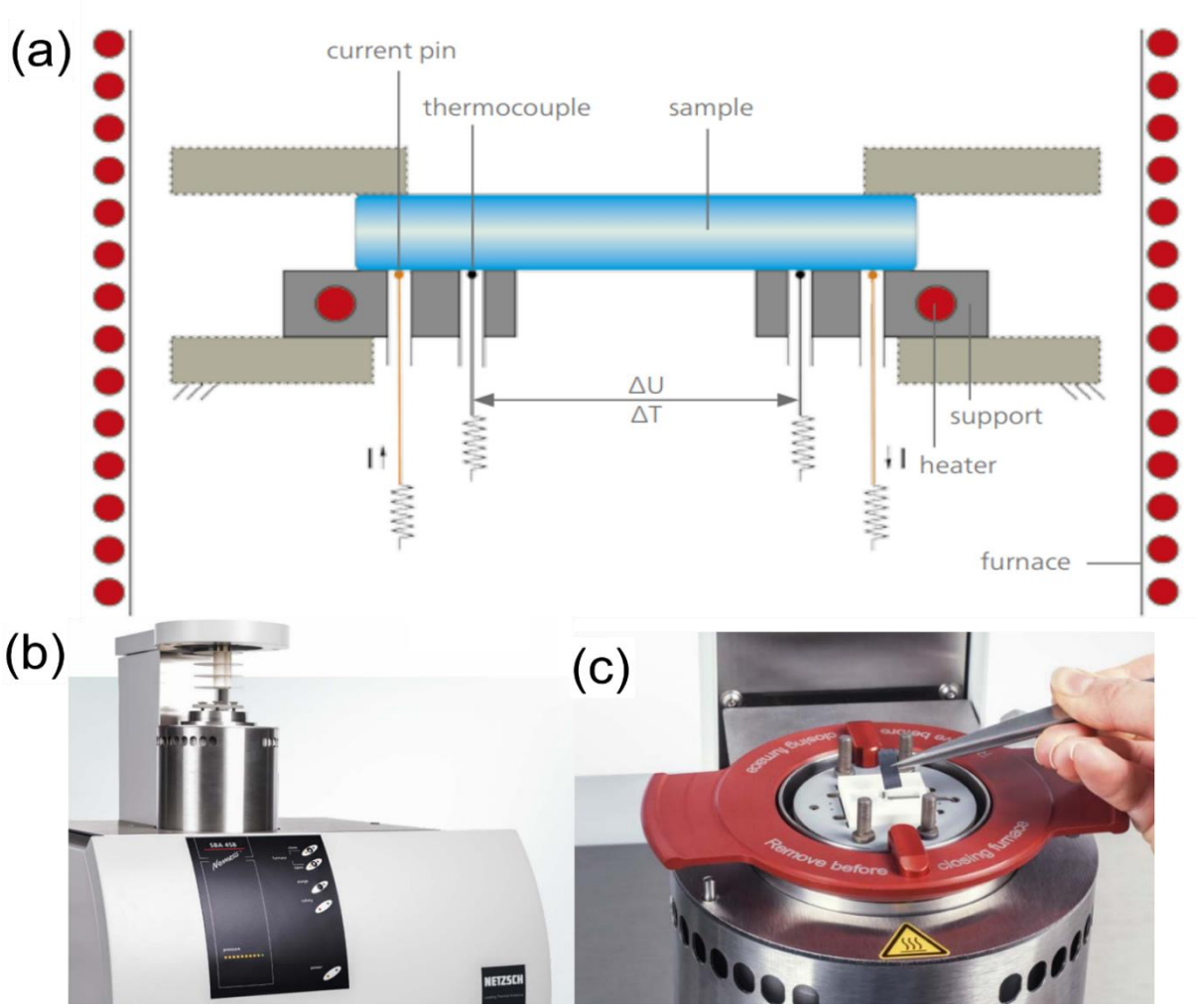


**Fig. R1.** Schematic illustration of SBA458 working mechanism and photos of laboratory equipment. (a) Schematic of working mechanism in SBA 458. (b) Non-loaded SBA 458 in the laboratory. (c) Loaded SBA 458 in the laboratory.

***Comment 3:*** *Combining inorganic materials with high thermoelectric properties and flexible conductive materials is a feasible strategy to develop flexible thermoelectric materials, a good case of Chem. Eng. J. 320 (2017) 201-210 should be referred.*

**Response:** We have cited the mentioned article as the reference [51] of the revised manuscript."

**Response to Reviewer #3**

***General comment:*** *In this manuscript, the authors prepared an PEDOT:PSS/inorganic hybrid material with excellent thermoelectric performance originating from so-called interfacial engineering. This conception is intriguing. However, the discussion is weak and incomplete, especially for the variation of Seebeck coefficient of the hybrid materials. Furthermore, the carrier transportation between interfaces is barely discussed, not to mention the optimization process. The relation between material design and thermoelectric performance is not well established. I didn't recommend this current work to be published in Chemical Engineering Journal until a completion of a number of appropriate amendments according to the following points.*

***Comment 1:*** *What's the basic principle to optimize the carrier transportation in the interfacial region between organic and inorganic materials? If introducing a more conductive coating or element is fine, why copper is selected instead of other noble elements?*

**Response:** We appreciate the constructive comments from the reviewer. The basic principle to optimize interfacial carriers transport between organic and inorganic materials lies in the reduction of interfacial contact resistance to prevent intense interfacial carrier scatterings.[1-3] Cu coating towards BST fillers is initially designed based on below two reasons. Firstly, Cu exhibits outstanding electrical conductivity, which holds great promises to reduce the interfacial contact resistance and carrier scatterings. Secondly, Cu coating towards BST thermoelectric materials has been confirmed to result in the significant boost of electrical properties by our previous works.[4, 5] Considering this, Cu-BST fillers are promising to have increased hybrid thermoelectric performances than single BST fillers. Other coatings using noble metals such as Ag and Ni are also promising and deserve our future studies.

***Comment 2:*** *In this case there is a CuTe phase between PEDOT:PSS and BST according to the HRTEM and XRD results, i.e., two interfacial region may exist in this hybrid system: one laid between PEDOT crystalline and CuTe, and another laid between CuTe and BST. Structure characterization is well presented. But the carrier transport between these interfaces is barely discussed. A more solid experimental evidence or mathematical model should be provided to quantitatively illustrate that the carrier transportation between these interfaces has been optimized.*

**Response:** As-claimed optimization of interfacial carrier transports mainly occurs between polymers and fillers, which is at the interface between BST and PEDOT before Cu coatings, and CuTe and PEDOT after Cu coatings. It is not critical to consider the interface between CuTe and BST, as our study utilized chemical coating and Cu-BST as the filler is considered as a whole, whose thermoelectric performances are suggested in **Fig. S1** in the **Supporting Information**.

In order to manifest the optimization of interfacial carrier transports between polymers and fillers. Experimentally, boosted system electrical conductivity in **Fig. 4a** and increased carrier mobilities in **Table 1** are observed. Theoretically, we also calculate series- and parallel-connection models of hybrid films and compare with our experimental results, which are added to the **Supporting Information**. Specifically, parallel- and series-connection model are given as[6, 7]

$$\sigma_{\text{parallel}} = \sigma_{\text{PEDOT}}(1-x) + \sigma_{\text{filler}}x\,, \tag{1}$$

$$S_{\text{parallel}} = \frac{(1-x)\sigma_{\text{PEDOT}}S_{\text{PEDOT}} + x\sigma_{\text{filler}}S_{\text{filler}}}{(1-x)\sigma_{\text{PEDOT}} + x\sigma_{\text{filler}}}\,, \tag{2}$$

$$\sigma_{\text{series}} = \frac{\sigma_{\text{filler}}\sigma_{\text{PEDOT}}}{\sigma_{\text{filler}}(1-x) + \sigma_{\text{PEDOT}}x}\,, \text{ and} \tag{3}$$

$$S_{\text{series}} = \frac{S_{\text{filler}}\kappa_{\text{PEDOT}}x + S_{\text{PEDOT}}\kappa_{\text{filler}}(1-x)}{\kappa_{\text{PEDOT}}x + \kappa_{\text{filler}}(1-x)}, \tag{4}$$

where *x* is the volume fraction of fillers. We compare the calculation results with experimental results with 4*wt*. % filler content, and the results are shown in **Fig. R2** (**Fig. S3** in the **Supporting Information**).

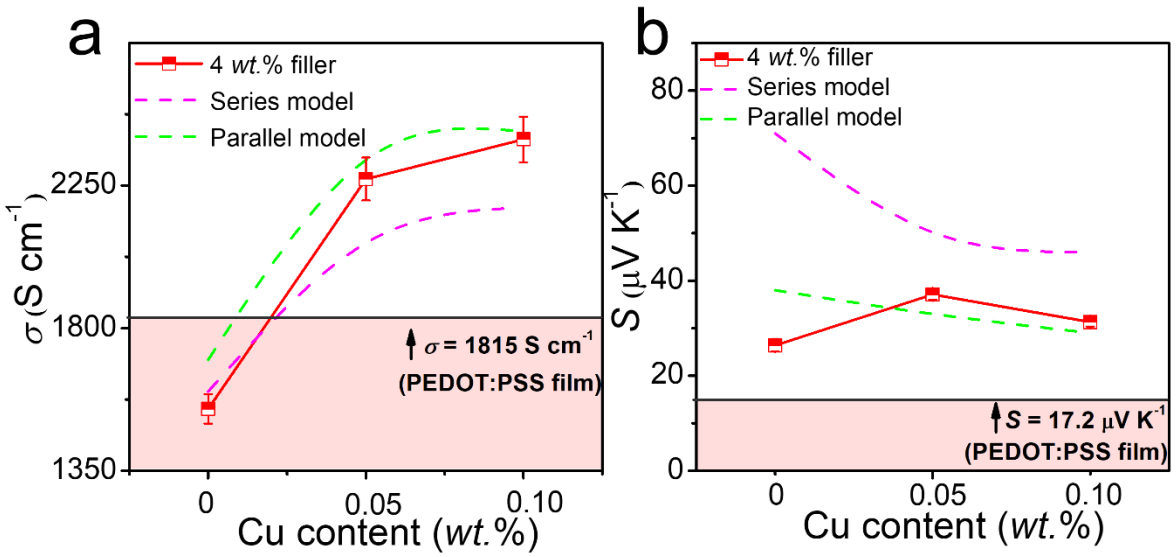


**Fig. R2.** Experimental (a) electrical conductivity and (b) Seebeck coefficient of 4*wt*. % filler content hybrid film compared with calculation results of series- and parallel-models.

Without Cu coating, both the electrical conductivity and Seebeck coefficient lie beyond the prediction range. This can be understood as that most carriers are scattered at the interface, deteriorating system electrical properties. After Cu coating, the system shows reasonable results within the prediction range, which indicates the "blocking" effects of fillers are mitigated due to reduced interfacial contact resistance. This contrast supports our claim of optimized interfacial transport.

Relevant discussions have been added to **Page 14** of the revised manuscript as "To manifest above claims, series- and parallel-connection models are employed to predict $\sigma$ and $S$ of hybrid films with 4*wt*. % filler content and compare with our experimental results. The results are illustrated in **Fig. S3**. Without Cu coating, both $\sigma$ and $S$ lie beyond the prediction range. This

can be understood as that most carriers are scattered at the interface, deteriorating system electrical properties. After Cu coating, the system shows reasonable results within the prediction range, which indicates the "blocking" effects of fillers are mitigated due to reduced interfacial contact resistance. This contrast supports our claims of optimized interfacial transport."

***Comment 3:*** *Table 1 presented that the mobility and concentration of carrier of hybrid materials simultaneously increased with the introduction of Cu. Yet based on the Boltzmann transportation theory model, the Seebeck coefficient has a negative correlation with the carrier concentration. Meanwhile, the Seebeck coefficient of hybrid material with 4 wt% filler firstly increased and then dropped with the introduction of Cu. Authors should give a further explanation on this variation and clarify what kind of role did CuTe layer play in this variation.*

**Response:** The increase of carrier concentration is caused by Cu introduction into the hybrid system. This is underpinned by **Fig. S1c**, where significantly boosted carrier concentrations are observed after Cu coatings. The enhancement of system carrier mobility, on the other hand, stems from reduced interfacial contact resistance induced by CuTe layer, where less carriers are scattered during the interfacial transports.

Relevant discussions have been added on **Page 16** of the revised manuscript as "Hall measurements are applied to investigate the change of system carrier concentration ($n$) and $\mu$ before and after Cu coatings, and **Table 1** summarizes the results. $n$ is observed to improve from ~8.06 to ~8.28 and ~8.37 × $10^{20}$ $cm^{-3}$ after Cu coatings, which is caused by the introduction of Cu, as manifested by $n$ of BST before and after Cu coatings in **Figure S1c**. Effective increased $\mu$ occurs from ~13.72 to ~18.04 and ~18.82 $cm^2$ $V^{-1}$ $s^{-1}$ after Cu coatings. This verifies the optimization of interfacial carrier transports and accounts for increased $\sigma$."

The negative relationship between carrier concentration and Seebeck coefficient depicted by Boltzmann transportation theory model follows Pisarenko relation:[8]

$$S = \frac{8\pi^2 k_B^2}{3eh^2} m^* T \left(\frac{\pi}{3n}\right)^{2/3}, \quad (5)$$

where $k_B$, $h$ and $m^*$ are the Boltzmann constant, the Planck constant, and the density of states (DOS) effective mass, respectively. However, such a relationship is proposed based on the assumption that carriers are delocalized.[9] These are inconsistent with carrier transports and structures of conductive polymers.[10] Specifically, conductive polymers can be structurally considered as highly conductive crystalline domains surrounded by poorly conductive amorphous matrices.[11, 12] Crystalline domains within conductive polymers possess ordered stackings of rigid conjugated chains from π-π interactions, leading to the relatively unimpeded transport of electrons,[13-15] while amorphous domains exhibit localized electrons transport, due to significantly dampened carrier mobility from amorphous chain stacking.[13] Therefore, Pisarenko relation is not thoroughly applicable for conductive polymers.

Actually, the variation of Seebeck coefficient in our study can be explained by the interfacial energy filtering effect between polymer matrix and inorganic fillers.[16-19] Specifically, carriers tend to be severely scattered at the interface without CuTe layer (no interfacial energy filtering), while passing through fillers with CuTe layer due to reduced interfacial contact resistance, inducing the interfacial energy filtering. This explains the increase of Seebeck coefficient after Cu coating. With increasing the amount of Cu coating, Cu-BST filler presents reduced Seebeck coefficient due to increased carrier concentration, as shown in **Fig. S1b** and **c** in the **Supporting Information**, leading to slightly dropped system Seebeck coefficient.

Relevant discussion has been modified on **Page 16** of the revised manuscript as "On the other hand, it should be noted that Cu-BST fillers (both 0.05 *wt*.% and 0.1 *wt*.%) possess more obvious boost towards *S* compared with BST fillers. This may because introduced CuTe layers reduce interfacial contact resistance, allowing more carriers to transport through BST fillers to induce more sufficient interfacial energy filtering. With the increasing amount of Cu coating, *S* of Cu-BST fillers reduces due to increased *n*, as show in **Figure S1b** and **c**, which consequently leads to slightly dropped system *S*."

***Comment 4:*** *There is poor discussion on the band diagram in Figure 4b. How did the authors get the band structure basically involving LOMO, HOMO and EF of the hybrid materials or individual components? What's the meaning of this diagram? Did this relate to interfacial-engineering? Why a high average energy is favorable to a high Seebeck coefficient?*

**Response:** The band structure of hybrid is schematically plotted based on work functions and Fermi levels locations of each individual component. Specifically, in the hybrid system, system Fermi level is firstly assumed at one energy level.[16-18] Then the positions of LOMO and HOMO for polymers or CB and VB for inorganic fillers are plotted based on their relative positions to their own Fermi levels. Finally, based on the energy offset between filler VB and polymer HOMO, the interfacial energy barrier is determined.

The meaning of this plot is to schematically illustrate the interfacial energy filtering process occurred at the interfaces, which accounts for the increase of system Seebeck coefficient. Interfacial energy filtering of carriers as one important process at the interface is related to interfacial engineering.

The relationship between Seebeck coefficient and carrier energy can be explained in the below way. For degenerately doped thermoelectric materials, Seebeck coefficient as a function of the energy dependence of the electrical conductivity follows Mott relation[20]

$$S = \frac{\pi^2}{3}\frac{k_B^2 T}{e}\left\{\frac{d[\ln(\sigma(E))]}{dE}\right\}_{E=E_{l'}} , \quad (6)$$

where $k_B$ is the Boltzmann constant. Meanwhile, taken at the Fermi energy for degenerate semiconductors, or at any value of $E$ and integrated over energy in the general case, electrical conductivity can be described as

$$\sigma = ne\mu = \frac{ne^2\tau}{m^*} , \quad (7)$$

where $m^*$ is the effective mass and $\tau$ is the relaxation time, which can be further described as

$$\tau = \tau_0 E^{\lambda-\frac{1}{2}}, \quad (8)$$

where λ is the scattering parameter, typically λ =0 for scattering of electrons by acoustic phonons, and λ =2 for scattering of electrons by ionized impurities.[21] The trend can be found that with higher carrier energy $E$ obtained, $\tau$ can be boosted, leading to higher $\sigma$ and accordingly higher $S$.[22]

***Comment 5:*** *According to XRD results in Figure 3(a), PEDOT crystalline occurred after pre- and post-treatment. Yet in Figure 3(d), authors insisted that the fringe pattern is inorganic filler. Why it can't be the PEDOT crystalline?*

**Response:** The ordering effect towards conductive polymers by pre- and post-treatments leads to lamella stacking in the microstructure (enhanced crystallinity). However, as can be seen from the cross-sectional SEM images in **Fig. 3b**, the distance between stackings should be tens of nanometre, while the *d*-spacing in **Fig. 3d** is less than 1 nm. Therefore, the fringe pattern should reflect inorganic filler rather than PEDOT crystalline.

**Response to Reviewer #4**

***General comment:*** *In this study, the authors reported a new methodology to optimize the interfacial carriers transport in $Bi_{0.5}Sb_{1.5}Te_3$/PEDOT:PSS composite, by coating $Bi_{0.5}Sb_{1.5}Te_3$ fillers with highly conductive CuTe layer. Due to synergistic improvements of electrical conductivity and Seebeck coefficient, a promising electrical conductivity of ~2300 S $cm^{-1}$ and impressive power factor of 312 μW $m^{-1}$ $K^{-2}$ have been achieved at room temperature. Moreover, a home-made flexible thermoelectric device has been fabricated to generate a open-circuit thermovoltage of ~7.7 mV with the human wrist as the thermal source.*

*Basically, this work is a comprehensive study with systematic analysis and discussions. The observed boosted interfacial carriers transport and record power factor of 312 μW $m^{-1}K^{-2}$ might be of great interest to researchers of inorganic/organic flexible thermoelectric field. Additionally, as-fabricated flexible thermoelectric generator shows full potentials to generate electricity with human body, which could be novel for thermoelectric clothes developments. Therefore, I suggest to accept this paper for publication after the consideration of the following minor issues:*

***Comment 1:*** *In terms of $Bi_{0.5}Sb_{1.5}Te_3$ filler size, the inset BSE image of Figure 2b shows the size of several hundreds of nanometres. However, the TEM image of 6 wt.% Cu-BST/PEDOT:PSS film in Figure 3d indicates filler size less than 100 nm. How would you explain this?*

**Response:** We appreciate the positive comments from the reviewer. The smaller $Bi_{0.5}Sb_{1.5}Te_3$ filler size observed in **Fig. 3d** than **Fig. 2b** can be attributed to blocking effects of conductive polymers towards TEM electron beams, where partial lattice structures of inorganic fillers underneath conductive polymers cannot be observed.

One typical SEM image of as-prepared $Bi_{0.5}Sb_{1.5}Te_3$ fillers is provided in **Fig. R3** (**Fig. S2** in the **Supporting Information**). It can be found filler size is ~400 nm, which is consistent with **Fig. 2b**.

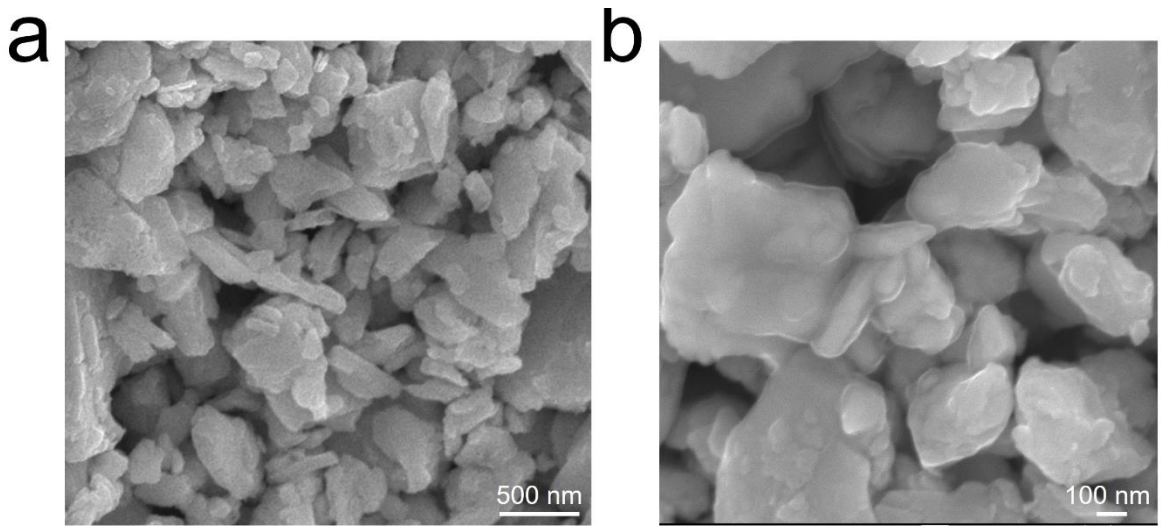


**Fig. R3**. Typical SEM images of as-prepared $Bi_{0.5}Sb_{1.5}Te_3$ fillers.

Relative discussions have been added to **Page 13** of the revised manuscript as "It should be noted that the size of fillers in our study are typically ~400 nm, as shown in **Fig. S2**. The smaller filler size observed in **Fig. 3d** can be attributed to blocking effects of conductive polymers towards TEM electron beams, where partial lattice structures of inorganic fillers underneath conductive polymers cannot be observed."

***Comment 2:*** *As described by the experimental section, conductive polymer PEDOT:PSS was treated sequentially by pre- and post-treatments to increase the crystallinity. During the post-treatments, PEDOT:PSS needs to be fabricated into films in order to be immersed into concentrated $H_2SO_4$. In this case, how can PEDOT:PSS be incorporated with fillers later to prepare the TE ink?*

**Response:** PEDOT:PSS films after DMSO pre-treatment and concentrated $H_2SO_4$ post-treatment are transformed into PEDOT:PSS slurry by intensively stirring films overnight on

the magnetic stir plate. The uniform TE ink is then prepared by thoroughly mixing PEDOT:PSS slurry with $Bi_{0.5}Sb_{1.5}Te_3$ fillers. Relevant discussions can be found in **Experimental Section** as "The as-treated PEDOT:PSS films were lastly magnetically stirred into PEDOT:PSS slurry, which was ready for the film fabrication."

***Comment 3:*** *The authors ascribed the improvements of Seebeck coefficient to interfacial energy filtering effects, which is reasonable. However, only filtering effects between BST and PEDOT:PSS are considered. Why the effects of as-coated highly conductive CuTe layer are neglected?*

**Response:** The interfacial energy filtering effect of CuTe is neglected in our study considering the following two reasons. Firstly, as manifested by high-magnitude TEM images of BST fillers in **Fig. 2**, as-coated CuTe layer is only ~17 nm, whose tiny amount can be neglected compared with ~400 nm BST fillers. Secondly, CuTe presents alloy-like electrical properties with the Fermi level deeply lying in the valance band, whose capacity to filter holes during the transport is quite rare, which can be ignored.

**Reference**

[1] B. Zhang, J. Sun, H.E. Katz, F. Fang, R.L. Opila, Promising Thermoelectric Properties of Commercial PEDOT:PSS Materials and Their $Bi_2Te_3$ Powder Composites, ACS Applied Materials & Interfaces 2 (2010) 3170-3178.

[2] X.B. Zhao, S.H. Hu, M.J. Zhao, T.J. Zhu, Thermoelectric properties of Bi0.5Sb1.5Te3/polyaniline hybrids prepared by mechanical blending, Materials Letters 52 (2002) 147-149.

[3] N. Toshima, N. Jiravanichanun, H. Marutani, Organic Thermoelectric Materials Composed of Conducting Polymers and Metal Nanoparticles, Journal of Electronic Materials 41 (2012) 1735-1742.

[4] Z. Huang, H. Zhang, K. Zheng, X. Dai, Y. Yu, H. Cheng, F. Zu, Z.-G. Chen, Enhancing thermoelectric performance of Cu-modified Bi0.5Sb1.5Te3 by electroless plating and annealing, Progress in Natural Science: Materials International 28 (2018) 218-224.

[5] Z. Huang, X. Dai, Y. Yu, C. Zhou, F. Zu, Enhanced thermoelectric properties of p-type Bi 0.5 Sb 1.5 Te 3 bulk alloys by electroless plating with Cu and annealing, Scripta Materialia 118 (2016) 19-23.

[6] L. Wang, Z. Zhang, Y. Liu, B. Wang, L. Fang, J. Qiu, K. Zhang, S. Wang, Exceptional thermoelectric properties of flexible organic−inorganic hybrids with monodispersed and periodic nanophase, Nature Communications 9 (2018) 3817.

[7] H. Ju, J. Kim, Chemically Exfoliated SnSe Nanosheets and Their SnSe/Poly(3,4-ethylenedioxythiophene):Poly(styrenesulfonate) Composite Films for Polymer Based Thermoelectric Applications, ACS Nano 10 (2016) 5730-5739.

[8] R. Moshwan, L. Yang, J. Zou, Z.-G. Chen, Eco-Friendly SnTe Thermoelectric Materials: Progress and Future Challenges, 27 (2017) 1703278.

[9] J. Zhou, X. Li, G. Chen, R. Yang, Semiclassical model for thermoelectric transport in nanocomposites, Physical Review B 82 (2010) 115308.

[10] S.D. Kang, G.J. Snyder, Charge-transport model for conducting polymers, Nature Materials 16 (2017) 252-257.

[11] A.J. Epstein, J.M. Ginder, F. Zuo, H.S. Woo, D.B. Tanner, A.F. Richter, M. Angelopoulos, W.S. Huang, A.G. MacDiarmid, Insulator-to-Metal Transition in Polyaniline Effect of Protonation in Emeraldine, Synthetic Met 21 (1987) 63-70.

[12] P. Sheng, J. Klafter, Hopping Conductivity in Granular Disordered Systems, Phys Rev B 27 (1983) 2583-2586.

[13] O. Bubnova, X. Crispin, Towards Polymer-Based OrganicThermoelectric Generators, Energy Environ. Sci. 5 (2012) 9345.

[14] P.J. Brown, D.S. Thomas, A. Köhler, J.S. Wilson, J.-S. Kim, C.M. Ramsdale, H. Sirringhaus, R.H. Friend, Effect of Interchain Interactions on the Absorption and Emission of Poly(3-hexylthiophene), Phys Rev B 67 (2003) 064203.

[15] C.A. Hunter, J.K.M. Sanders, The Nature of π-π Interactions, J Am Chem Soc 112 (1990) 5525-5534.

[16] M. He, J. Ge, Z. Lin, X. Feng, X. Wang, H. Lu, Y. Yang, F. Qiu, Thermopower enhancement in conducting polymer nanocomposites via carrier energy scattering at the organic–inorganic semiconductor interface, Energy & Environmental Science 5 (2012) 8351.

[17] C. Gayner, Y. Amouyal, Energy Filtering of Charge Carriers: Current Trends, Challenges, and Prospects for Thermoelectric Materials, Advanced Functional Materials (2019) 1901789.

[18] J. Choi, J.Y. Lee, S.-S. Lee, C.R. Park, H. Kim, High-Performance Thermoelectric Paper Based on Double Carrier-Filtering Processes at Nanowire Heterojunctions, Advanced Energy Materials 6 (2016) 1502181.

[19] Z. Liang, M.J. Boland, K. Butrouna, D.R. Strachan, K.R. Graham, Increased power factors of organic–inorganic nanocomposite thermoelectric materials and the role of energy filtering, Journal of Materials Chemistry A 5 (2017) 15891-15900.

[20] N.F. Mott, E.A. Davis, Electronic Processes in Non-crystalline Materials, Oxford, Clarendon, 1979.

[21] J.P. Heremans, C.M. Thrush, D.T. Morelli, Thermopower enhancement in PbTe with Pb precipitates, Journal of Applied Physics 98 (2005) 063703.

[22] J.P. Heremans, C.M. Thrush, D.T. Morelli, Thermopower enhancement in lead telluride nanostructures, Physical Review B 70 (2004) 115334.

Graphical Abstract

# TOC

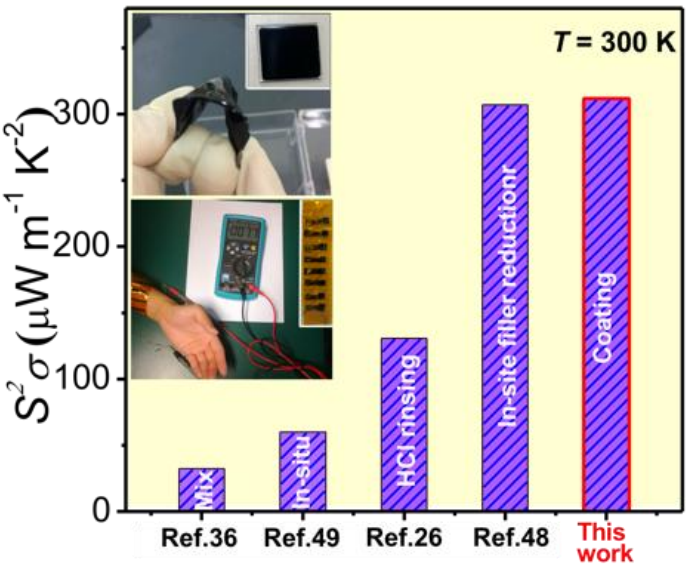

**Highlight:**

• Facilely realizing the boost of interfacial carrier transports.

• Effectively coating $Bi_{0.5}Sb_{1.5}Te_3$ fillers with highly conductive CuTe layer.

• Achieving highly crystallized PEDOT:PSS as the matrix.

• Producing promising $\sigma$ of ~2300 S $cm^{-1}$ and peak $S^2\sigma$ of 312 μW $m^{-1}$ $K^{-2}$ at room temperature. • Generating promising open-circuit thermovoltage of ~7.7 mV with human wrist as the thermal source.

# $Bi_{0.5}Sb_{1.5}Te_3$/PEDOT:PSS-Based Flexible Thermoelectric Film and Device

*Yuan Wang,*[a,b] *Min Hong,*[a,b] *Wei-Di Liu,*[b] *Xiao-Lei Shi,*[a,b] *Sheng-Duo Xu,*[b] *Qiang Sun,*[b] *Han Gao,*[b] *Siyu Lu,*[c] *Jin Zou,*[b,d] *Zhi-Gang Chen**[,a,b]

[a]Centre for Future Materials, University of Southern Queensland, Springfield Central, Queensland 4300, Australia.

[b]School of Mechanical and Mining Engineering, The University of Queensland, Brisbane, Queensland 4072, Australia.

[c]College of Chemistry and Molecular Engineering, Zhengzhou University, Zhengzhou, 450001, China;

[d]Centre for Microscopy and Microanalysis, The University of Queensland, Brisbane, Queensland 4072, Australia.

[*]Corresponding author. Email: zhigang.chen@usq.edu.au (ZGC); zhigang.chen@uq.edu.au (ZGC)

**Abstract**

Incorporating inorganic thermoelectric fillers into conductive polymers is one promising strategy to develop high-performance flexible thermoelectric films. However, due to the relatively high interfacial contact resistance between fillers and polymers, carriers tend to be scattered at the interfaces during the interfacial transports, which deteriorates the electrical properties of the system, and in turn leads to low energy conversion efficiency. Here, a new strategy is developed to optimize interfacial carrier transports in $Bi_{0.5}Sb_{1.5}Te_3$/PEDOT:PSS composite, by coating $Bi_{0.5}Sb_{1.5}Te_3$ fillers with highly conductive CuTe layer. With highly crystallized PEDOT:PSS prepared as the matrix, high-performance Cu-$Bi_{0.5}Sb_{1.5}Te_3$ /PEDOT:PSS film is fabricated with promising $\sigma$ of ~2300 S $cm^{-1}$ and peak $S^2\sigma$ of 312 μW $m^{-1}$ $K^{-2}$ at room temperature, which reaches to a record-high value in the reported $Bi_{0.5}Sb_{1.5}Te_3$/PEDOT:PSS composites. Accordingly, a home-made flexible thermoelectric device is fabricated using our prepared composites, generating a promising open-circuit thermovoltage of ~7.7 mV with the human wrist as the thermal source. This study addresses the significance of interfacial carrier transport, hinting the bright prospects of cheap conductive polymers as the effective power source of wearable electronics.

***Keywords***: Thermoelectrics, Flexible, PEDOT:PSS, Bismuth telluride, Interface

## 1. Introduction

Rapid advances of the Internet of Things (IoT) spark the increasing developments of miniature and integrated wearable electronics, where conventional batteries as the power source have severe disadvantages such as frequent replacements/recharge and extra maintenance.[1, 2] Flexible thermoelectric (FTE) materials enable the direct power generation from heat through the Seebeck effect and can present conformal interactions with heat sources to maximize heat harvesting, which can, therefore, act as energy-autonomous, maintenance-free and emission-free power sources for wearable electronics.[3] To evaluate the power generation efficiency of FTE materials, a dimensionless figure of merit ($zT$) is defined as: $zT = S^2\sigma T/\kappa$, where $S$, $\sigma$, $\kappa$, and $T$ is the Seebeck coefficient, electrical conductivity, thermal conductivity, and operating temperature, respectively.[4] Promising $zT$ can thus be effectively contributed by high power factor ($S^2\sigma$) and low $\kappa$. Currently, studies on FTE materials mainly focus on conductive polymers, such as poly(3,4-ethylenedioxythiophene)-poly(styrenesulfonate) (PEDOT:PSS),[5-8] poly(3-hexylthiophene-2,5-diyl) (P3HT),[9-11] and polyaniline (PANI),[12-16] due to their intrinsic flexibility and low $\kappa$. However, their poor electrical properties result in inferior $S^2\sigma$ than inorganic TE materials, which restricts their $zT$ improvements. In this regard, optimizing the electrical properties of conductive polymers is of vital significance.

So far, several strategies have been used to increase $S^2\sigma$ of conductive polymers. For example, improved $\sigma$ of PEDOT:PSS can be realized from ordered microstructure or improved crystallinity after polar solvents pre-treatments with dimethyl sulfoxide (DMSO)[17, 18] or ethylene glycol (EG),[19-21] or concentrated $H_2SO_4$ post-treatments.[8, 22] $S$ can be effectively tuned with controlled oxidation levels of conductive polymers, by means of reducing PEDOT-Tos film in the

tetrakis(dimethylamino)ethylene (TDAE) atmosphere,[23] or immersing PEDOT:PSS film in reducing $NaBH_4$,[24] NaOH[5] and $N_2H_4$[24] solutions.

Additionally, incorporating inorganic TE fillers into conductive polymers matrix has also been proposed to be an effective strategy to boost $S^2\sigma$,[25-29] where FTE composites might be synergistically endowed with decent $S^2\sigma$ of inorganic TE fillers and low $\kappa$ of conductive polymers. So far, FTE composites mainly focus on PEDOT:PSS as the polymer matrix, due to its promising $\sigma$ of 4380 S $cm^{-1}$ at room temperature,[22] abundance, and facile processability, which may be beneficial for scale-up productions. Inorganic TE fillers mainly include $Bi_2Te_3$[26, 29, 30] and $Bi_{0.5}Sb_{1.5}Te_3$ (BST)[25] considering their decent low-temperature $S^2\sigma$, or Te[27, 31, 32] and SnSe[33] due to their outstanding low-temperature $S$. Effectively enhanced $S^2\sigma$ of 32.26 μW $m^{-1}$ $K^{-1}$ has been witnessed from BST/PEDOT:PSS composite, which presents more than three times higher value than pristine PEDOT:PSS film.[25] In spite of the progress, $S^2\sigma$ of FTE composite is still much inferior to inorganic TE materials, possibly caused by the overlook of interfacial carrier transports between fillers and polymers, which significantly restrains contributions of fillers to $S^2\sigma$. By applying surface engineering to inorganic fillers, interfacial carrier transports can be optimized, and in turn, further boost of $S^2\sigma$ becomes possible.[26, 30] Typically, Zhang *et al.*[26] applied HCl rinsing to remove the potential oxidation layer on the surface of *p*-type $Bi_2Te_3$ filler to optimize interfacial carrier transports, and found significantly increased $S^2\sigma$ of 131 μW $m^{-1}$ $K^{-1}$ in the $Bi_2Te_3$/PEDOT:PSS film, compared with that of 35.6 μW $m^{-1}$ $K^{-1}$ without HCl rinsing. Recently, Goo *et al.*[30] conducted proton-irradiation treatments on the surface of $Bi_2Te_3$ fillers, which intentionally induced surface defect sites as the extra adsorption sites for polymer chains, and in turn led to intensified interfacial interactions. Consequently, an outstanding $S^2\sigma$ of 325.3 μW $m^{-1}$ $K^{-1}$ was achieved in the $Bi_2Te_3$/PEDOT:PSS film,[30] which is among the top values of

$Bi_2Te_3$/PEDOT:PSS composites. Therefore, surface engineering of fillers is a promising approach in securing splendid $S^2\sigma$ in FTE composites.

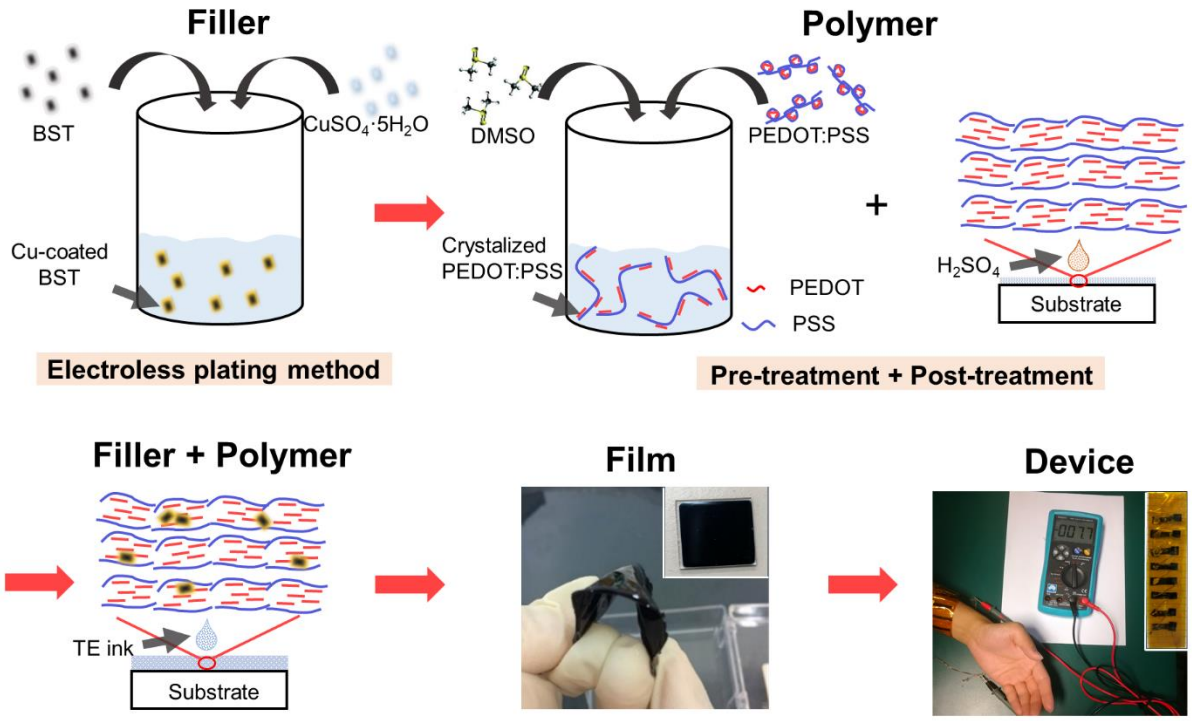


**Fig. 1.** Schematic illustration of the processes to fabrication Cu-BST/PEDOT:PSS FTE films and device.

In this study, we develop a new strategy to optimize interfacial carrier transports in the BST/PEDOT:PSS composite, by coating BST fillers with highly conductive CuTe layer ($\sigma$>5.2×10$^5$ S cm$^{-1}$).[34] With highly crystallized PEDOT:PSS prepared as the matrix, superhigh-performance Cu-BST/PEDOT:PSS film was fabricated and showed promising $\sigma$ of 2270 S cm$^{-1}$ and peak $S^2\sigma$ of 312 μW m$^{-1}$ K$^{-1}$ at room temperature, which reached to state-of-the-art values reported for BST/PEDOT:PSS composites.[25, 26, 35, 36] **Fig. 1** schematically depicts the fabrication process of the composites, where fillers and polymers are separately prepared. Cu-BST fillers were synthesized by a facile electroless plating method.[37, 38] Crystallized PEDOT:PSS was obtained

through DMSO polar solvent pre-treatments, followed by concentrated $H_2SO_4$ post-treatment to selectively remove insulating PSS, which in turn render increased $\sigma$. Finally, the BST/PEDOT:PSS film with decent flexibility was fabricated by drop-casting TE ink onto a pre-cleaned glass substrate. A home-made FTE device was fabricated accordingly, showing the effective power generation with the human wrist as the thermal source.

## 2. Experimental section

### *2.1 Materials*

Analytical grade Bi shots (99.999%), Sb shots (99.999%), Te shots (99.999%) and NaOH (99.999%) were purchased from Alfa-Aesar (United States) and used without any further purifications. PEDOT:PSS aqueous solution (Clevios PH1000) was purchased from Heraeus (Germany). Dimethyl sulfoxide (DMSO), concentrated $H_2SO_4$ (98%), concentrated $HNO_3$ (98%), copper sulfate pentahydrate, formaldehyde, Ethylenediaminetetraacetic acid disodium salt (EDTA-2Na) and polyvinylidene difluoride (PVDF) membrane filter (0.45 μm pore size) were all purchased from Sigma-Aldrich (Australia).

### *2.2 Synthesis of Cu-coated BST fillers*

High-purity Bi shots (99.999%), Sb shots (99.999%) and Te shots (99.999%) were weighted based on the nominal composition of BST, and subsequently sealed into a quartz tube under the vacuum of $10^{-3}$ Pa. The quartz tube was then placed in the furnace, where the precursors were melted and kept for 10 h at 1023 K. As-synthesized BST ingot was finally ball-milled (AXT, 8000M) for 20 min under 15 Hz in order to obtain fine BST fillers.

As-prepared BST fillers were then coated with Cu using facile electroless plating method. Specifically, BST fillers were firstly sonicated in 5% $HNO_3$ solution for 1 h, followed by deionized water rinsing for at least three times to remove residual impurities. Afterwards, pretreated BST

fillers were transferred into the coating solution consisting of copper sulfate pentahydrate as the copper source, formaldehyde as the reducing agent, EDTA-2Na as the complex agents and NaOH to provide the alkaline environment. The coating process was conducted under the sonication and lasted for 1 h at 330 K. The as-coated BST fillers were alternatively washed by deionized water and ethonal for at least three times, before being collected by centrifugation and dried at 330 K in the oven overnight. The as-collected Cu-BST fillers were ultimately reduced under $H_2$ atmosphere at 580 K for 1 h, and naturally cooled down to the room temperature. The as-reduced Cu-BST fillers were sealed in the vacuum and ready for the next step.

*2.3 Treatments of PEDOT:PSS conductive polymers*

Aqueous solution PEDOT:PSS was firstly mixed with 10 *vol*.% polar solvent DMSO and sonicated for 6 h at 330 K. The solution was then filtered by PVDF membrane (0.45 μm pore size) using vacuum-assisted filtration method to remove insulating and hydrophilic PSS. The filtrate was collected and magnetically stirred until forming the PEDOT:PSS slurry, which was subsequently drop casted onto pre-cleaned silicon dioxide substrates, and later dried at 330 K for 20 min on the heating plate. PEDOT:PSS films were then immersed into concentrated $H_2SO_4$ (98%) for 10 h to further remove insulating PSS, and rinsed with deionized water for three times afterwards. The as-treated PEDOT:PSS films were lastly magnetically stirred into PEDOT:PSS slurry, which was ready for the film fabrication.

*2.4 Fabrication of Cu-BST/PEDOT:PSS films*

Silicon dioxide substrates were pre-cleaned following the sequence of detergent, deionized water, ethanol and plasma cleaning. PEDOT:PSS slurry was mixed with different amount of Cu-BST fillers (2 *wt*.%, 4 *wt*.% and 6 *wt*.%) and sonicated for 6 h, followed by intense magnetic stirring for another 6 h at room temperature to obtain uniform Cu-BST/PEDOT:PSS inks. BST fillers

without Cu coating were also mixed with PEDOT:PSS slurry following above processes as the contrast set. 100 μL ink was subsequently drop casted onto pre-cleaned silicon dioxide substrates, and later dried at 330 K for 20 min on the heating plate. The as-fabricated films were collected and showed decent flexibility.

*2.5 Fabrication of FTE device*

10 milliliters of as-prepared inks was paved in the glass petri dish with the diameter of 55 mm. After drying at 330 K for 2 hours, as-fabricated film was immersed in ethanol to detach from the glass petri dish. Free-standing Cu-BST/PEDOT:PSS films were obtained by collecting detached film and drying at 330 K for 20 min. As-obtained films were cut into rectangular pieces with the size of 25 × 8 $mm^2$, which were subsequently connected by copper wires and assembled into FTE device using polyimide as the substrate Two polyimide films were lastly used to cover top and bottom of the FTE device, acting as the protection layer.

*2.6 Measurements and characterization*

Electrical properties of as-fabricated films, including $\sigma$ and $S$, were measured by SBA458 (Netzsch) at 300 K. X-ray diffraction (XRD, Bruker-D8) was applied to determine the crystal structure of BST fillers before and after Cu coatings. Grazing incidence XRD (GIXRD, Rigaku SmartLab) was utilized to investigate the crystallinity of conductive polymers before and after treatments. Scanning electron microscopy (SEM, JEOL JSM-7100F) and transmission electron microscopy (TEM, TECNAI-F20) were utilized to study the morphology and structural characteristics. X-ray energy-dispersive spectroscopy (EDS) mapping and spot analysis (equipped in HITACHI-SU3500 SEM) were conducted to confirm the successful surface coating of Cu on the BST fillers.

**3. Results and discussion**

**Fig. 2** shows the structural characterizations of BST fillers before and after Cu coating. **Fig. 2a** is XRD patterns taken from BST, 0.05 *wt*.% Cu-BST and 0.1 *wt*.% Cu-BST fillers, respectively. As can be seen, the diffraction peaks of the as-synthesized BST powders can be exclusively indexed as hexagonal structured BST with lattice parameters of $a$ = 4.28424 nm and $c$ = 30.52389 nm and a space group of $R\bar{3}$m (PDF#49-1713). After Cu coating, additional peaks at $2\theta$ of $12.8^0$, $25.4^0$ and $31.1^0$ emerge in the diffraction peaks of 0.05 *wt*.% Cu-BST, which can be precisely retrieved as orthorhombic structured CuTe with lattice parameters of $a$ = 3.16 nm, b = 4.08 nm and $c$ = 6.93 nm and a space group *P*mmn (PDF#22-0252). This indicates that Cu reacts with BST particles during the coating process to form CuTe. **Fig. 2b** shows the EDS results, and further confirms the successful coating of Cu on the surface of BST particles, where Cu is detected from EDS spot analysis and clearly observed on the boundaries of BST particles from the EDS maps. **Fig. 2c-g** are TEM results to clarify the insights of the coating process. As can be seen, the uncoated BST particles (**Fig. 2c**) show relatively smooth boundaries, while zig-zag boundaries appear in the coated BST particles (**Fig. 2d**), which is attributed to the $HNO_3$ pre-treatments to generate sufficient reaction sites for maximum Cu coating. As verified in **Fig. 2d** and **e,** CuTe is clearly observed on BST boundaries, which is consistent with SEM EDS maps, shown in **Fig. 2b**. **Fig. 2e** shows typical high-resolution TEM image, in which the as-coated CuTe layer is relatively uniform with a thickness of 17 nm. **Fig. 2f** is its corresponding high-angle annular dark-field (HAADF) image of the interface, where the CuTe layer with small atomic mass shows dark contrast compared with the bright contrast of the BST particle. **Fig. 2g** is a zoom-in high-resolution TEM (HRTEM) image taken from the CuTe layer (highlighted by red square in **Fig. 2e**), in which two sets of lattice planes with $d$-spacing of 0.18 and 0.23 nm can be detected with the angle of $50.3^0$ that correspond to the (022) and (102) atomic planes of CuTe, respectively.

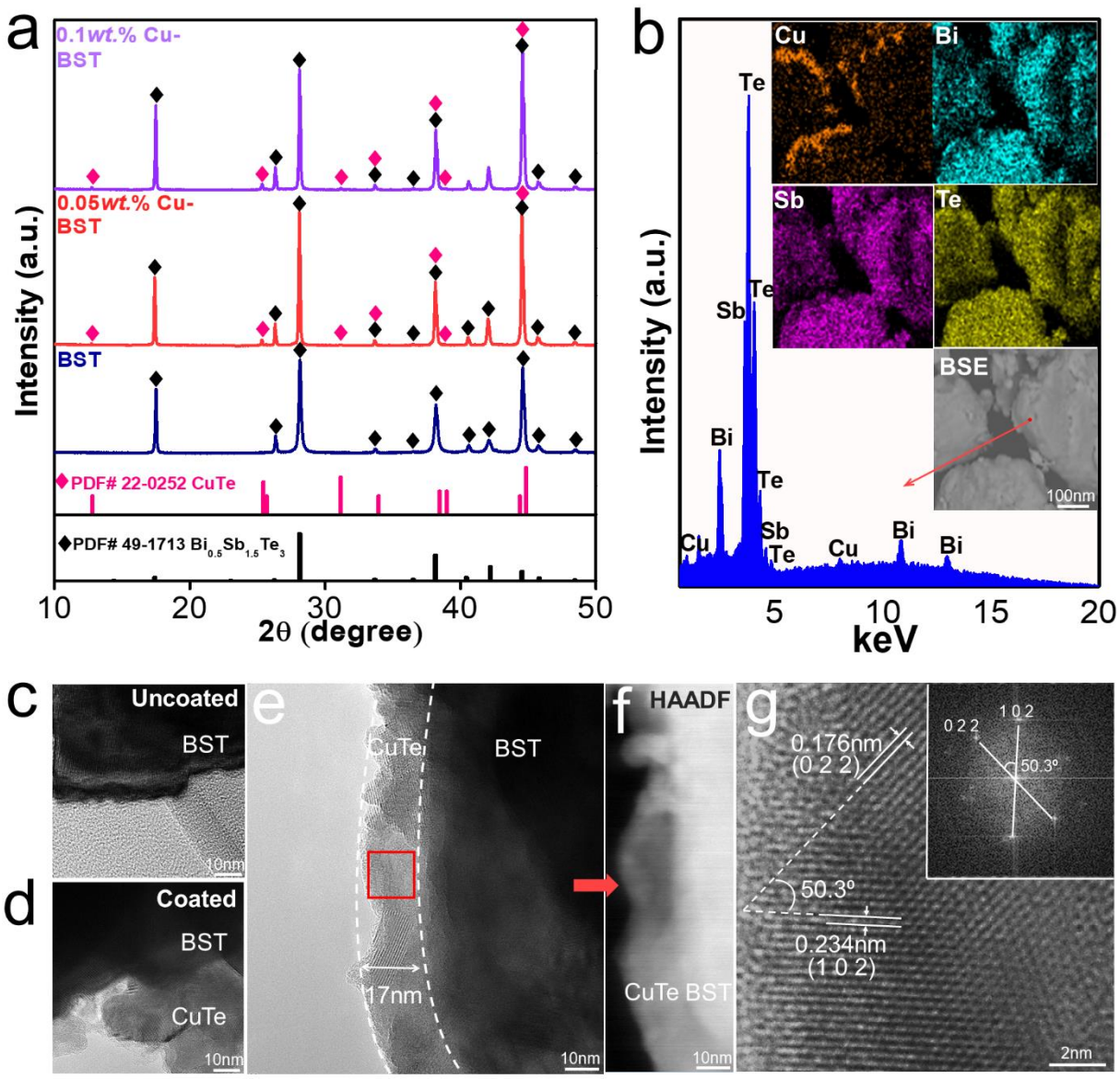


**Fig. 2.** (a) XRD patterns of BST, 0.05 *wt*.% Cu-BST and 0.1 *wt*.% Cu-BST fillers. (b) EDS spot spectrum of 0.1 *wt*.% Cu-BST fillers with the inset of mappings of Cu, Bi, Sb and Te. Typical high-magnitude TEM images of BST fillers (c) before and (d) (e) after Cu coating, together with corresponding (f) HAADF and (g) HRTEM images.

It has been reported that high crystallinity of PEDOT:PSS can lead to high $\sigma$,[22] while selectively removal of insulating PSS can induce improved crystallinity of PEDOT:PSS.[39] Here, we applied

DMSO-$H_2SO_4$ double treatments to effectively remove insulating PSS and in turn result in highly crystallized PEDOT:PSS. **Fig. 3a** shows XRD patterns of PEDOT:PSS films before and after the treatments. The pristine film shows weak peaks at low $2\theta$ of 3.3 and $7^o$ corresponding to the lamella stacking of alternate PEDOT and PSS along the (100) plane, and high $2\theta$ of 18 and $26^0$, which can be attributed to amorphous PSS and inter-chain planar stacking along the (010) planes.[40] The weak intensities of all diffraction peaks indicate the amorphous microstructure and low crystallinity of pristine PEDOT:PSS film. These form a sharp contrast with DMSO-$H_2SO_4$ treated PEDOT:PSS film, where two sharp diffraction peaks at ~7 and $12.5^0$ indicate that (100) stacking has been greatly intensified after the treatment. Moreover, it should be noted that two peaks of (100) stacking both exhibit an obvious right peak shift after the treatment, which is from the original $2\theta$ of 3.3 and $7^0$ to ~7 and $12.5^0$, respectively. According to Bragg's law,[8] this hints the shrink of spacing between (100) stackings, which confirms the effective removal of insulating PSS. On the other hand, two peaks of (010) planes stacking are still quite weak after the treatment, and present ignorable intensities compared with two peaks of (010) stacking. This means (100) stacking dominates in the microstructure of treated film, which contributes to highly crystallized PEDOT:PSS. Increased crystallinity of PEDOT:PSS is also associated with chemical structure transition of PEDOT monomers from benzoid to quinoid after DMSO-$H_2SO_4$ double treatments,[41, 42] as shown in **Fig. 3a**. PEDOT monomers with benzoid structure are connected by relatively flexible C-C bonds, which tend to induce deviations of adjacent thiophene rings and formation of coiled-up conformation.[43] However, PEDOT monomers with quinoid structure are connected by rigid π bonds (C=C bonds), which is favored by flat PEDOT backbones and in turn enhanced crystallinity.[42] Cross-sectional SEM images of PEDOT:PSS films of **Fig. 3b** further confirm the

improved crystallinity, where lamella stacking is clearly visible after the treatment. Additionally, the decreased thickness of film from 4 to 2.5 μm verifies the PSS depletion.

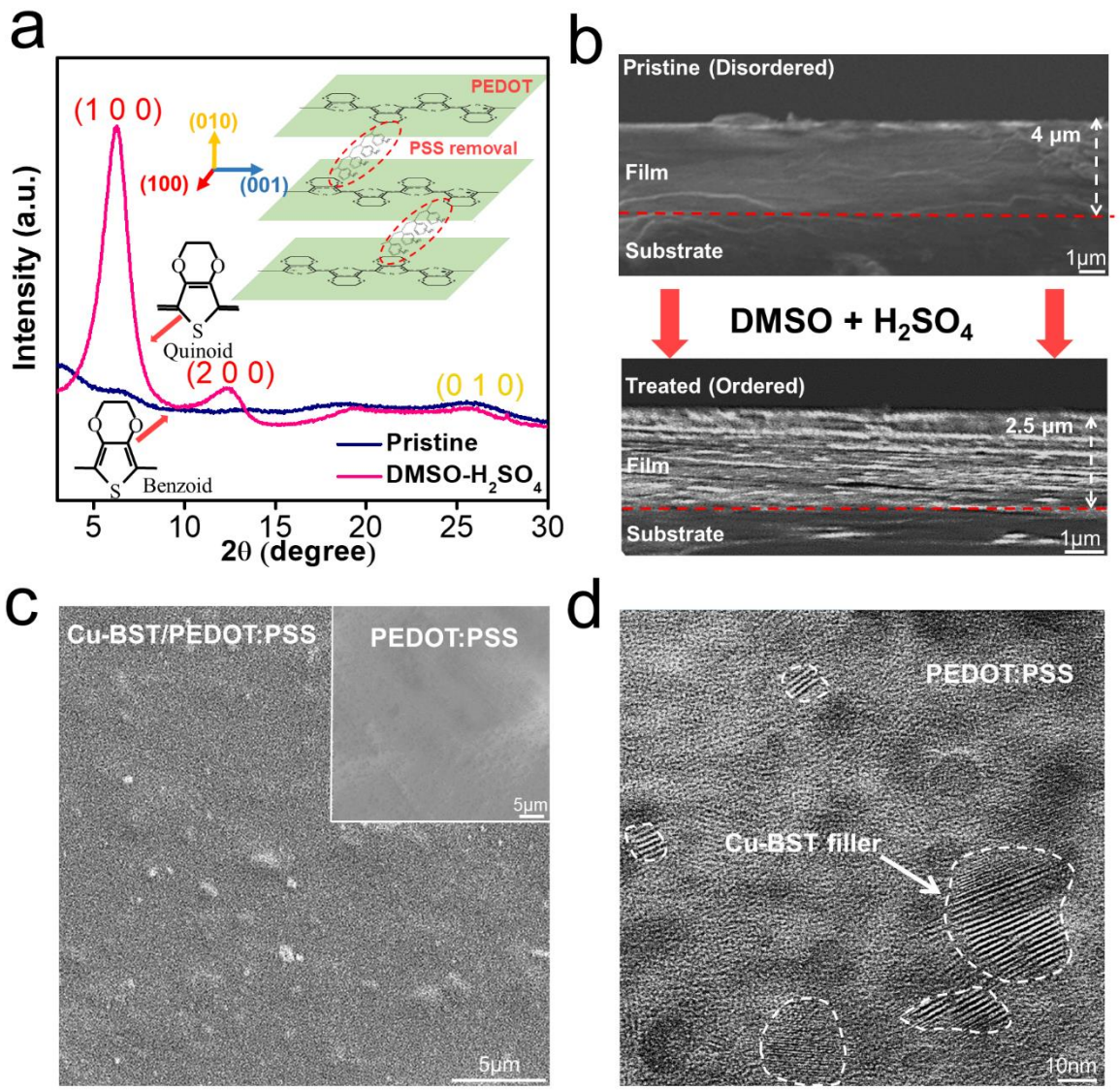


**Fig. 3.** (a) XRD patterns and (b) cross-sectional SEM images of PEDOT:PSS films before and after DMSO-$H_2SO_4$ double treatments. (c) Typical top-view SEM and (d) TEM images of PEDOT:PSS films with 6 *wt*.% Cu-BST filler incorporation, with the inset of (c) showing PEDOT:PSS film without fillers.

With Cu-coated BST fillers and crystallized PEDOT:PSS conductive polymer, Cu-BST/PEDOT:PSS film was fabricated. **Fig. 3c** shows the typical top-view SEM image of the film, with the inset of PEDOT:PSS film without fillers. Relatively uniform dispersion of fillers can be observed, and the introduction of fillers results in the improved roughness of the films. **Fig. 3d** is a TEM image, and further confirms the well dispersion of fillers. It should be noted that the size of fillers in our study are typically ~400 nm, as shown in **Fig. S2**. The smaller filler size observed in **Fig. 3d** can be attributed to blocking effects of conductive polymers towards TEM electron beams, where partial lattice structures of inorganic fillers underneath conductive polymers cannot be observed. Moreover, PEDOT:PSS is observed to closely envelop Cu-BST fillers, which can be beneficial to optimize the interfacial carrier transport.

**Fig. 4** plots the room-temperature $\sigma$ and $S$ of the as-fabricated films. **Fig. 4a** shows DMSO-$H_2SO_4$ treated PEDOT:PSS films, in which decent $\sigma$ of 1815 S cm$^{-1}$ is achieved, which is ascribed to the as-obtained high crystallinity. This value agrees with reported crystalline PEDOT:PSS.[8, 22] With filler incorporations, it is found that pristine BST fillers can deteriorate $\sigma$, showing values lower than treated PEDOT:PSS films. On one hand, this may be due to the lower $\sigma$ value of pristine BST fillers (~ 500 S cm$^{-1}$, **Fig. S1a**) than treated PEDOT:PSS. On the other hand, the surface of pristine BST fillers can potentially scatter carriers during the transport due to the relatively high interfacial contact resistance, which leads to the depressed carrier mobility ($\mu$) and in turn low $\sigma$.

With introducing highly conductive CuTe interfacial layers, $\sigma$ can be significantly enhanced and exceed that of treated PEDOT:PSS films under various filler contents. Such a tendency is more obvious with increasing the Cu coating, and an outstanding $\sigma$ value of 2520 S cm$^{-1}$ is achieved in the 0.1 *wt*.% Cu-BST/PEDOT:PSS film with 2 *wt*.% filler content. Such a $\sigma$ improvement can be attributed to high $\sigma$ value of the CuTe layers ($\sigma$>5.2×10$^5$ S cm$^{-1}$),[34] as well as the optimized

interfacial carriers transport, as schematically depicted in **Fig. 4b**. In contrast to the carrier blocking effect induced by pristine BST fillers, highly conductive CuTe interfacial layers can render carriers to travel through BST fillers, rather than being scattered. In this way, optimized interfacial carriers transport with improved $\mu$ is generated, which is favorable by high $\sigma$. To manifest above claims, series- and parallel-connection models are employed to predict $\sigma$ and $S$ of hybrid films with 4*wt*. % filler content and compare with our experimental results. The results are illustrated in **Fig. S3**. Without Cu coating, both $\sigma$ and $S$ lie beyond the prediction range. This can be understood as that most carriers are scattered at the interface, deteriorating system electrical properties. After Cu coating, the system shows reasonable results within the prediction range, which indicates the "blocking" effects of fillers are mitigated due to reduced interfacial contact resistance. This contrast supports our claims of optimized interfacial transport.

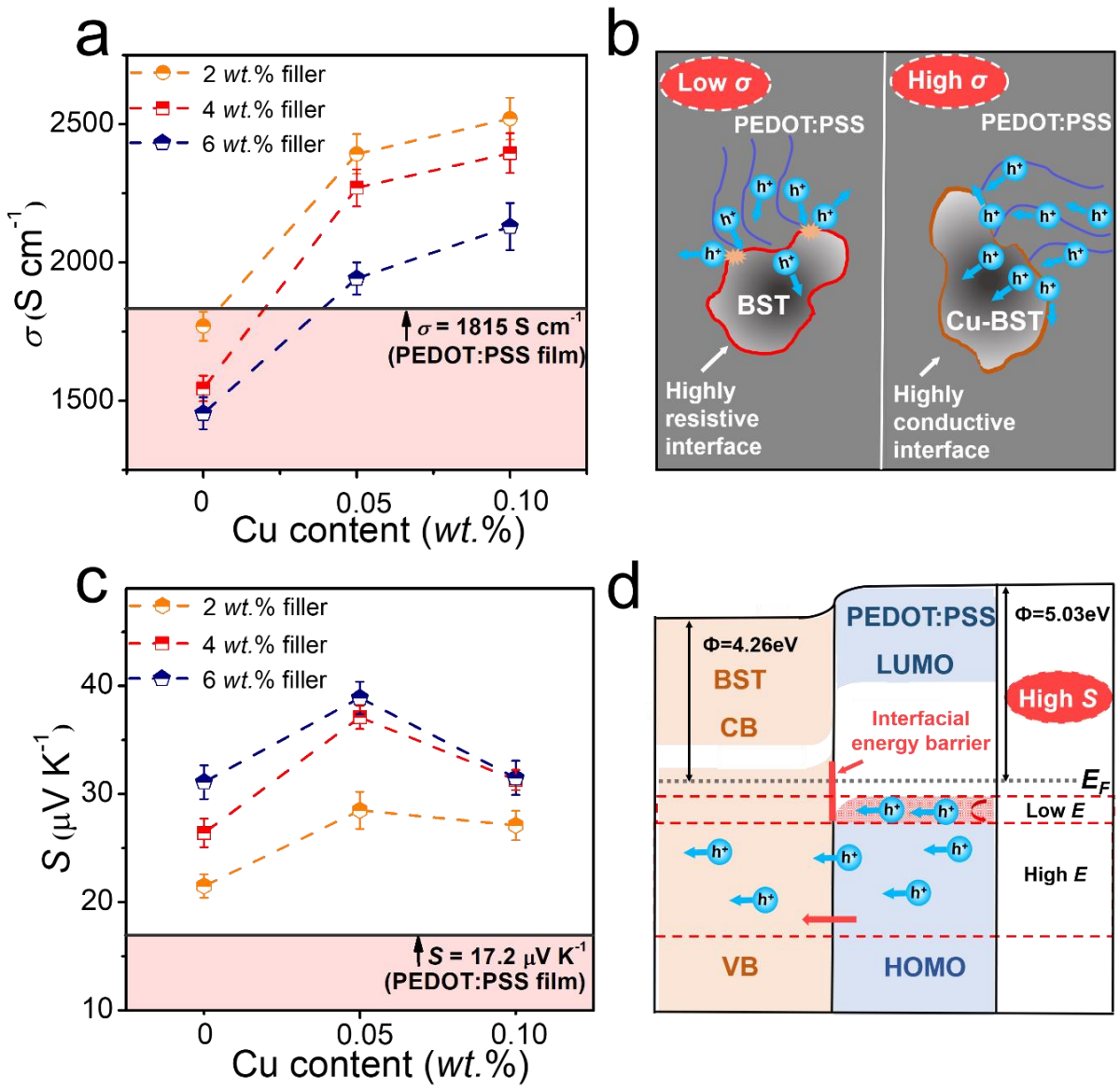


**Fig. 4.** Measured room-temperature (a) $\sigma$ and (c) $S$ of PEDOT:PSS films incorporated with BST fillers before and after Cu coatings (filler content 2 *wt*.%, 4 *wt*.% and 6 *wt*.%), with corresponding schematics of (b) optimized interfacial carrier transports and (d) interfacial energy filtering.

**Table 1**. ***n*** **and** ***μ*** **of BST/PEDOT:PSS films before and after Cu coatings (4** ***wt*****.% filler).**

| Parameter | BST/PEDOT:PSS | 0.05 *wt*.% Cu-BST/PEDOT:PSS | 0.1 *wt*.% Cu-BST/PEDOT:PSS |
|---|---|---|---|
| $\mu$ ($cm^2\ V^{-1}\ s^{-1}$) | 13.72±1.96 | 18.04±2.21 | 18.82±2.82 |
| $n$ ($10^{20}\ cm^{-3}$) | 8.06±1.21 | 8.29±1.24 | 8.37±1.19 |

Hall measurements are applied to investigate the change of carrier concentration ($n$) and $\mu$ before and after Cu coatings, and **Table 1** summarizes the results. $n$ is observed to improve from ~8.06 to ~8.28 and ~8.37 × $10^{20}$ $cm^{-3}$ after Cu coatings, which is caused by the introduction of Cu, as manifested by $n$ of BST before and after Cu coatings in **Fig. S1c**. Effective increased $\mu$ occurs from ~13.72 to ~18.04 and ~18.82 $cm^2$ $V^{-1}$ $s^{-1}$ after Cu coatings. This verifies the optimization of interfacial carrier transports and accounts for increased $\sigma$. Additionally, high filler contents are found to cause low $\sigma$. This agrees with other reports,[44, 45] and stems from more introduced interfaces between polymers and fillers.

In terms of $S$, **Fig. 4c** shows that additions of fillers before and after Cu coatings both show positive effects. Peak $S$ of 38.9 μV $K^{-1}$ can be achieved from 0.05 *wt*.% Cu-BST/PEDOT:PSS films with 6 *wt*.% filler content. The $S$ improvement is contributed by the interfacial energy filtering effect,[46, 47] as shown in **Fig. 4d**. With the interfacial energy offset existing between PEDOT:PSS and BST fillers, an interfacial energy barrier can be formed between the highest occupied molecular orbital (HOMO) of PEDOT:PSS and valance band (VB) of BST fillers. Carriers (holes) with relatively low energy tend to be scattered at the interfaces while those with high energy pass through. Therefore, the average energy of system carriers is improved, which is favored by high $S$.[47] On the other hand, it should be noted that Cu-BST fillers (both 0.05 *wt*.% and 0.1 *wt*.%) possess boosted $S$ compared with BST fillers. This may because introduced CuTe layers reduce interfacial contact resistance, allowing more carriers to transport through BST fillers to induce more sufficient interfacial energy filtering. With increasing the amount of Cu coating, $S$ of Cu-BST fillers reduces due to increased $n$, as shown in **Fig. S1b** and **c**, which consequently leads to slightly dropped $S$.

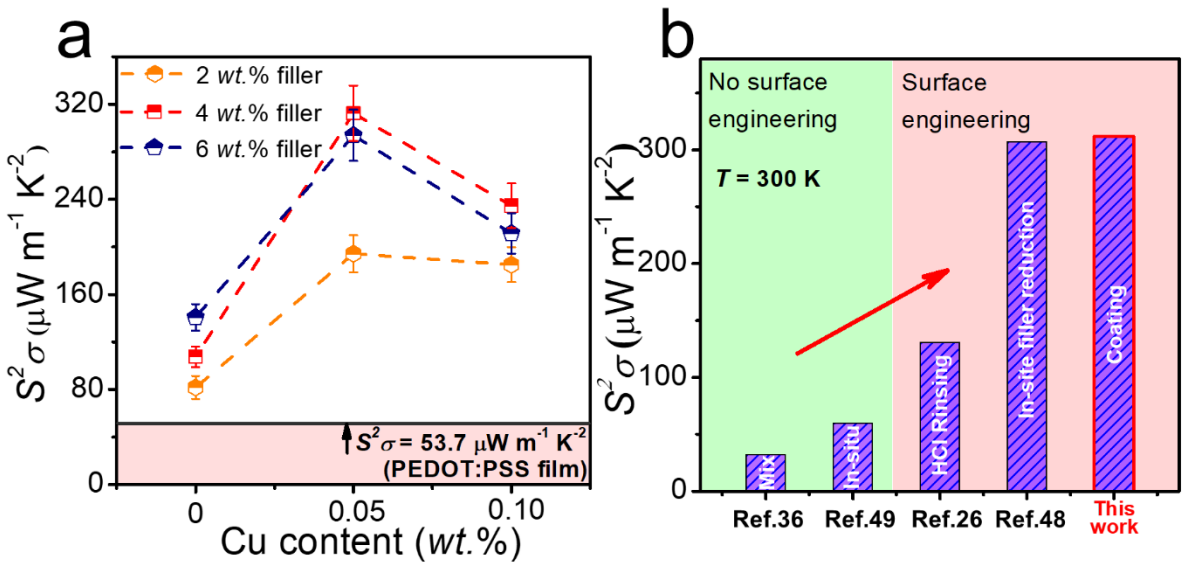


**Fig. 5.** (a) Measured room-temperature $S^2\sigma$ of PEDOT:PSS films incorporated with BST fillers before and after Cu coatings (filler content 2 *wt*.%, 4 *wt*.% and 6 *wt*.%). (b) Comparisons of $S^2\sigma$ between this work and other reported BST/PEDOT:PSS works,[26, 36, 48, 49] where the potentials of filler surface engineering are visible.

With the measured $\sigma$ and $S$, $S^2\sigma$ is calculated and plotted in **Fig. 5a**. The $S^2\sigma$ enhancement induced by Cu coating is evident, and an outstanding $S^2\sigma$ value of 312 μW m$^{-1}$ K$^{-2}$ can be observed in the 0.05 *wt*.% Cu-BST/PEDOT:PSS film with 4 *wt*.% filler content, which exhibits almost six times improvements than our treated PEDOT:PSS film. Compared with other BST/PEDOT:PSS FTE works,[26, 36, 48, 49] **Fig. 5b** shows the outstanding performance of our strategy, in which significant $S^2\sigma$ enhancement is obtained after considerations of interfaces, manifesting surface engineering of fillers.

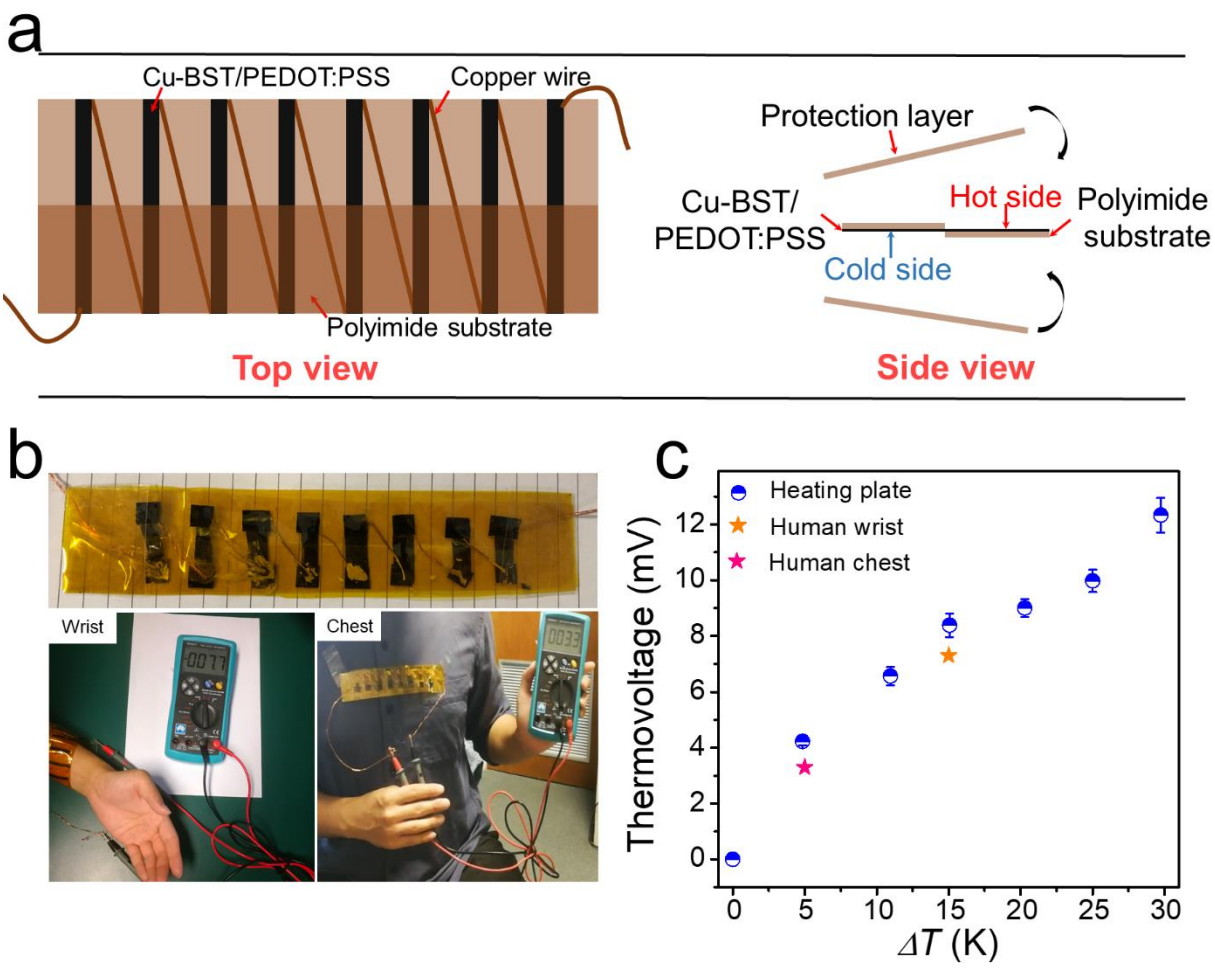


**Fig. 6.** (a) Schematic diagram of a home-made FTE device. (b) Images of the as-fabricated FTE device, and its thermovoltage generations with human wrist and chest as thermal sources. (c) Measured thermovoltages using heating plate, human wrist and chest as thermal sources.

To confirm the potentials of power generation using the as-prepared Cu-BST/PEDOT:PSS films, a home-made FTE device was fabricated based on the structure shown in **Fig. 6a**. TE legs with the size of 25 × 8 $mm^2$ were assembled into the flexible polyimide substrate and connected by copper wires. Another two polyimide films were applied as the protection layer to cover top and bottom of TE legs. **Fig. 6b** shows the as-fabricated FTE device, where thermovoltages can be effectively generated when attaching the device onto human wrist and chest.[50-54] By firmly attaching one end

of the device onto the heating plate and exposing the other end in the air, more temperature differences can be achieved from 5 to 30 K, generating increased thermovoltages, as shown in **Fig. 6c**. Peak thermovoltage of ~12.3 mV can be realized with 30 K temperature difference between two ends of the device. It should be noted that heating plate as the thermal source can contribute slightly higher voltages than human body. This should be due to the heat loss occurred at the interface between human skin and the device, leading to reduced temperature differences and in turn deteriorated voltage generations.

## 4. Conclusions

In summary, we fabricated superhigh-performance Cu-BST/PEDOT:PSS FTE films by coating BST fillers with a highly conductive CuTe layer ($\sigma$>5.2×10$^5$ S cm$^{-1}$) and preparing highly crystallized PEDOT:PSS conductive polymer. High $\sigma$ of 2270 S cm$^{-1}$ was achieved, which is attributed to the boosted interfacial carriers transport and crystallized PEDOT:PSS. Meanwhile, $S$ was enhanced by interfacial energy filtering, reaching value up to 37.1 μV K$^{-1}$. Systematic XRD, EDS, SEM and TEM results confirm the successful introduction of nanoscale CuTe layers and the accomplishment of highly crystallized PEDOT:PSS. Effectively improved $\sigma$ of the system after Cu coating manifests the optimization of interfacial carriers transport, which is further supported by Hall measurement results. As a result, an outstanding $S^2\sigma$ value of 312 μW m$^{-1}$ K$^{-2}$ was realized at the room temperature, which serves as a state-of-the-art value for BST/PEDOT:PSS FTE composites. Meanwhile, a FTE device was fabricated using the as-prepared Cu-BST/PEDOT:PSS films, generating a promising open-circuit thermovoltage of ~7.7 mV with the human wrist as the thermal source.

## Notes

The authors declare no competing financial interest.

**Acknowledgements**

This work was financially supported by the Australian Research Council. ZGC thanks the USQ start-up grant and strategic research grant. Microscopy Australia is acknowledged for providing characterization facilities.

**Supporting Information**

Supporting information of this article can be found online free of charge.

**References**

[1] Y. Wang, L. Yang, X. L. Shi, X. Shi, L. Chen, M. S. Dargusch, J. Zou, Z. G. Chen, Flexible thermoelectric materials and generators: challenges and innovations, Adv. Mater. 31 (2019) e1807916.

[2] B. Russ, A. Glaudell, J. J. Urban, M. L. Chabinyc, R. A. Segalman, Organic thermoelectric materials for energy harvesting and temperature control, Nat. Rev. Mater. 1 (2016) 16050.

[3] Y. Ding, Y. Qiu, K. Cai, Q. Yao, S. Chen, L. Chen, J. He, High performance n-type Ag2Se film on nylon membrane for flexible thermoelectric power generator, Nat. Commun. 10 (2019) 841.

[4] Z. G. Chen, G. Han, L. Yang, L. Cheng, J. Zou, Nanostructured thermoelectric Materials: Current Research and Future Challenge, Prog. Nat. Sci. 22 (2012) 535-549.

[5] Z. Fan, P. Li, D. Du, J. Ouyang, Significantly enhanced thermoelectric properties of PEDOT:PSS films through sequential post-treatments with common acids and bases, Adv. Energy Mater. 7 (2017) 1602116.

[6] N. Kim, S. Kee, S. H. Lee, B. H. Lee, Y. H. Kahng, Y.-R. Jo, B.-J. Kim, K. Lee, Highly conductive PEDOT:PSS nanofibrils induced by solution-processed crystallization, Adv. Mater. 26 (2014) 2268-2272.

[7] Q. Wei, M. Mukaida, Y. Naitoh, T. Ishida, Morphological change and mobility enhancement in PEDOT:PSS by adding co-solvents, Adv. Mater. 25 (2013) 2831-2836.

[8] S. Xu, M. Hong, X. L. Shi, Y. Wang, L. Ge, Y. Bai, L. Wang, M. Dargusch, J. Zou, Z. G. Chen, High-performance PEDOT:PSS flexible thermoelectric materials and their devices by triple post-treatments, *Chem. Mater.* 31 (2019) 5238-5244.

[9] Q. Zhang, Y. Sun, W. Xu, D. Zhu, Thermoelectric energy from flexible P3HT films doped with a ferric salt of triflimide anions, Energy Environ. Sci. 5 (2012) 9639-9644.

[10] L. Chen, W. Liu, Y. Yan, X. Su, S. Xiao, X. Lu, C. Uher, X. Tang, Fine-tuning the solid-state ordering and thermoelectric performance of regioregular P3HT analogues by sequential oxygen-substitution of carbon atoms along the alkyl side chains, *J. Mater. Chem. C* 7 (2019) 2333-2344.

[11] S. Qu, Q. Yao, L. Wang, Z. Chen, K. Xu, H. Zeng, W. Shi, T. Zhang, C. Uher, L. Chen, Highly anisotropic P3HT films with enhanced thermoelectric performance *via* organic small molecule epitaxy, NPG Asia Mater. 8 (2016) e292.

[12] Q. Yao, L. Chen, W. Zhang, S. Liufu, X. Chen, Enhanced thermoelectric performance of single-walled carbon nanotubes/polyaniline hybrid nanocomposites, ACS Nano 4 (2010) 2445-2451.

[13] H. Zengin, W. Zhou, J. Jin, R. Czerw, D. W. Smith Jr., L. Echegoyen, D. L. Carroll, S. H. Foulger, J. Ballato, Carbon nanotube doped polyaniline, Adv. Mater. 14 (2002) 1480-1483.

[14] Q. Yao, Q. Wang, L. Wang, L. Chen, Abnormally enhanced thermoelectric transport properties of SWNT/PANI hybrid films by the strengthened PANI molecular ordering, Energy Environ. Sci. 7 (2014) 3801-3807.

[15] Q. Yao, Q. Wang, L. Wang, Y. Wang, J. Sun, H. Zeng, Z. Jin, X. Huang, L. Chen, The synergic regulation of conductivity and Seebeck coefficient in pure polyaniline by chemically changing the ordered degree of molecular chains, J. Mater. Chem. A 2 (2014) 2634-2640.

[16] K. Lee, S. Cho, S. Heum Park, A. J. Heeger, C.-W. Lee, S. H. Lee, Metallic transport in polyaniline, Nature 441 (2006) 65-68.

[17] J. Ouyang, C.-W. Chu, F. C. Chen, Q. Xu, Y. Yang, High-conductivity poly(3,4-ethylenedioxythiophene):poly(styrene sulfonate) film and its application in polymer optoelectronic devices, Adv. Funct. Mater. 15 (2005) 203-208.

[18] Y. Xia, J. Ouyang, PEDOT:PSS films with significantly enhanced conductivities induced by preferential solvation with cosolvents and their application in polymer photovoltaic cells, J. Mater. Chem. 21 (2011) 4927-4936.

[19] G. H. Kim, L. Shao, K. Zhang, K. P. Pipe, Engineered doping of organic semiconductors for enhanced thermoelectric efficiency, Nat. Mater. 12 (2013) 719-723.

[20] J. Ouyang, Q. F. Xu, C. W. Chu, Y. Yang, G. Li, J. Shinar, On the mechanism of conductivity enhancement in poly (3,4-ethylenedioxythiophene): poly(styrene sulfonate) film through solvent treatment, Polymer 45 (2004) 8443-8450.

[21] J. Y. Kim, J. H. Jung, D. E. Lee, J. Joo, Enhancement of electrical conductivity of poly(3,4-ethylenedioxythiophene)/poly(4-styrenesulfonate) by a change of solvents, Synth. Metals 126 (2002) 311-316.

[22] N. Kim, S. Kee, S. H. Lee, B. H. Lee, Y. H. Kahng, Y. R. Jo, B. J. Kim, K. Lee, Highly conductive PEDOT:PSS nanofibrils induced by solution-processed crystallization, Adv. Mater. 26 (2014) 2268-2272.

[23] O. Bubnova, Z. U. Khan, A. Malti, S. Braun, M. Fahlman, M. Berggren, X. Crispin, Optimization of the thermoelectric figure of merit in the conducting polymer poly(3,4-ethylenedioxythiophene), *Nat. Mater.* 10 (2011) 429-433.

[24] N. Massonnet, A. Carella, O. Jaudouin, P. Rannou, G. Laval, C. Celle, J.-P. Simonato, Improvement of the Seebeck coefficient of PEDOT:PSS by chemical reduction combined with a novel method for its transfer using free-standing thin films, J. Mater. Chem. C 2 (2014) 1278-1283.

[25] Y. Du, K. F. Cai, S. Chen, P. Cizek, T. Lin, Facile preparation and thermoelectric properties of $Bi_2Te_3$ based alloy nanosheet/PEDOT:PSS composite films, ACS Appl. Mater. Interfaces 6 (2014) 5735-5743.

[26] B. Zhang, J. Sun, H. E. Katz, F. Fang, R. L. Opila, Promising thermoelectric properties of commercial PEDOT:PSS materials and their $Bi_2Te_3$ powder composites, ACS Appl. Mater. Interfaces 2 (2010) 3170-3178.

[27] D. Ni, H. Song, Y. Chen, K. Cai, Significantly enhanced thermoelectric performance of flexible PEDOT nanowire film *via* coating Te nanostructures, *J. Materiomics* (2019) doi.org/10.1016/j.jmat.2019.07.001.

[28] K. C. See, J. P. Feser, C. E. Chen, A. Majumdar, J. J. Urban, R. A. Segalman, Water-processable polymer-nanocrystal hybrids for thermoelectrics, Nano Lett. 10 (2010) 4664-4667.

[29] L. Wang, Z. Zhang, Y. Liu, B. Wang, L. Fang, J. Qiu, K. Zhang, S. Wang, Exceptional thermoelectric properties of flexible organic−inorganic hybrids with monodispersed and periodic nanophase, Nature Commun. 9 (2018) 3817.

[30] G. Goo, G. Anoop, S. Unithrattil, W. S. Kim, H. J. Lee, H. B. Kim, M. H. Jung, J. Park, H. C. Ko, J. Y. Jo, Proton- irradiation effects on the thermoelectric properties of flexible $Bi_2Te_3$/PEDOT:PSS composite films, Adv. Electron. Mater. 5 (2019) 1800786.

[31] Y. Lu, Y. Qiu, Q. Jiang, K. Cai, Y. Du, H. Song, M. Gao, C. Huang, J. He, D. Hu, Preparation and characterization of Te/Poly(3,4-ethylenedioxythiophene):Poly(styrenesulfonate)/$Cu_7Te_4$ ternary composite films for flexible thermoelectric power generator, ACS Appl. Mater. Interfaces 10 (2018) 42310-42319.

[32] Q. Meng, Q. Jiang, K. Cai, L. Chen, Preparation and thermoelectric properties of PEDOT:PSS coated Te nanorod/PEDOT:PSS composite films, Org. Electron. 64 (2019) 79-85.

[33] H. Ju, J. Kim, Chemically exfoliated SnSe nanosheets and their SnSe/Poly(3,4-ethylenedioxythiophene):Poly(styrenesulfonate) composite films for polymer based thermoelectric applications, ACS Nano 10 (2016) 5730-5739.

[34] D. Zhu, W. Huang, M. Song, M. Tu, Effects of annealing temperature on the electrical conductivity and mechanical property of Cu-Te alloys, J. Wuhan Uni. Tech.-Mater. Sci. Ed. 22 (2007) 88-90.

[35] J. H. We, S. J. Kim, B. J. Cho, Hybrid composite of screen-printed inorganic thermoelectric film and organic conducting polymer for flexible thermoelectric power generator, Energy 73 (2014) 506-512.

[36] M. Bharti, A. Singh, G. Saini, S. Saha, A. Bohra, Y. Kaneko, A. K. Debnath, K. P. Muthe, K. Marumoto, D. K. Aswal, S. C. Gadkari, Boosting thermoelectric power factor of free-standing

Poly(3,4ethylenedioxythiophene):polystyrenesulphonate films by incorporation of bismuth antimony telluride nanostructures, J. Power Sour. 435 (2019) 226758.

[37] S. Cao, Z. Y. Huang, F. Q. Zu, J. Xu, L. Yang, Z. G. Chen, Enhanced thermoelectric properties of Ag-modified $Bi_{0.5}Sb_{1.5}Te_3$ composites by a facile electroless plating method, ACS Appl. Mater. Interfaces 9 (2017) 36478-36482.

[38] Z. Huang, X. Dai, Y. Yu, C. Zhou, F. Zu, Enhanced thermoelectric properties of *p*-type $Bi_{0.5}Sb_{1.5}Te_3$ bulk alloys by electroless plating with Cu and annealing, Scr. Mater. 118 (2016) 19-23.

[39] Q. Zhang, Y. Sun, W. Xu, D. Zhu, Organic thermoelectric materials: emerging green energy materials converting heat to electricity directly and efficiently, Adv. Mater. 26 (2014) 6829-6851.

[40] K. E. Aasmundtveit, E. J. Samuelsen, L. A. A. Pettersson, O. Inganäs, T. Johansson, R. Feidenhans'l, Structure of thin films of poly(3,4-ethylenedioxythiophene), Synth. Metals 101 (1999) 561-564.

[41] R. Kroon, D. A. Mengistie, D. Kiefer, J. Hynynen, J. D. Ryan, L. Yu, C. Müller, Thermoelectric plastics: from design to synthesis, processing and structure–property relationships, Chem. Soc. Rev. 45 (2016) 6147-6164.

[42] O. Bubnova, X. Crispin, Towards polymer-based organic thermoelectric generators, Energy Environ. Sci. 5 (2012) 9345-9362.

[43] S. Garreau, G. Louarn, J. P. Buisson, G. Froyer, S. Lefrant, In-situ spectroelectrochemical raman studies of poly(3,4-ethylenedioxythiophene) (PEDT), Macromolecules 32 (1999) 6807-6812.

[44] M. He, J. Ge, Z. Lin, X. Feng, X. Wang, H. Lu, Y. Yang, F. Qiu, Thermopower enhancement in conducting polymer nanocomposites via carrier energy scattering at the organic–inorganic semiconductor interface, Energy Environ. Sci. 5 (2012) 8351.

[45] Z. Liang, M. J. Boland, K. Butrouna, D. R. Strachan, K. R. Graham, Increased power factors of organic–inorganic nanocomposite thermoelectric materials and the role of energy filtering, J. Mater. Chem. A 5 (2017) 15891-15900.

[46] J. Choi, J. Y. Lee, S.-S. Lee, C. R. Park, H. Kim, High-performance thermoelectric paper based on double carrier-filtering processes at nanowire heterojunctions, Adv. Energy Mater. 6 (2016) 1502181.

[47] C. Gayner, Y. Amouyal, Energy filtering of charge carriers: current trends, challenges, and prospects for thermoelectric materials, Adv. Funct. Mater. (2019) 1901789.

[48] J. Y. Lim, S. Cho, H. Kim, Y. Seo, Optimum thermoelectric performance of bismuth–antimony–telluride alloy/PEDOT:PSS nanocomposites prepared by an innovative redox process, ACS Appl. Energy Mater. (2019) 8219-8228.

[49] E. J. Bae, Y. H. Kang, K. S. Jang, C. Lee, S. Y. Cho, Solution synthesis of telluride-based nano-barbell structures coated with PEDOT:PSS for spray-printed thermoelectric generators, Nanoscale 8 (2016) 10885-10890.

[50] D. Bao, J. Chen, Y. Yu, W. Liu, L. Huang, G. Han, J. Tang, D. Zhou, L. Yang, Z.-G. Chen, Texture-dependent thermoelectric properties of nano-structured $Bi_2Te_3$, Chem. Eng. J. 388 (2020) 124295.

[51] C. Li, F. Jiang, C. Liu, W. Wang, X. Li, T. Wang, J. Xu, A simple thermoelectric device based on inorganic/organic composite thin film for energy harvesting, Chem. Eng. J. 320 (2017) 201-210.

[52] Y. Wang, W.-D. Liu, X.-L. Shi, M. Hong, L.-J. Wang, M. Li, H. Wang, J. Zou, Z.-G. Chen, Enhanced thermoelectric properties of nanostructured *n*-type $Bi_2Te_3$ by suppressing Te vacancy through non-equilibrium fast reaction, Chem. Eng. J. (2019) 123513.

[53] W.-D. Liu, L. Yang, Z.-G. Chen, J. Zou, Promising and eco-friendly $Cu_2X$-based thermoelectric materials: progress and applications, Adv. Mater. 32 (2020) 1905703.

[54] X.-L. Shi, X. Tao, J. Zou, Z.-G. Chen, High-performance thermoelectric SnSe: aqueous synthesis, innovations, and challenges, Adv. Sci. (2020) 1902923.

# $Bi_{0.5}Sb_{1.5}Te_3$/PEDOT:PSS-Based Flexible Thermoelectric Film and Device

*Yuan Wang,*[a,b] *Min Hong,*[a,b] *Wei-Di Liu,*[b] *Xiao-Lei Shi,*[a,b] *Sheng-Duo Xu,*[b] *Qiang Sun,*[b] *Han Gao,*[b] *Siyu Lu,*[c] *Jin Zou,*[b,d] *Zhi-Gang Chen*,*[a,b]

[a]Centre for Future Materials, University of Southern Queensland, Springfield Central, Queensland 4300, Australia.

[b]School of Mechanical and Mining Engineering, The University of Queensland, Brisbane, Queensland 4072, Australia.

[c]College of Chemistry and Molecular Engineering, Zhengzhou University, Zhengzhou, 450001, China;

[d]Centre for Microscopy and Microanalysis, The University of Queensland, Brisbane, Queensland 4072, Australia.

[*]Corresponding author. Email: zhigang.chen@usq.edu.au (ZGC); zhigang.chen@uq.edu.au (ZGC)

**Abstract**

Incorporating inorganic thermoelectric fillers into conductive polymers is one promising strategy to develop high-performance flexible thermoelectric films. However, due to the relatively high interfacial contact resistance between fillers and polymers, carriers tend to be scattered at the interfaces during the interfacial transports, which deteriorates the electrical properties of the system, and in turn leads to low energy conversion efficiency. Here, a new strategy is developed to optimize interfacial carrier transports in $Bi_{0.5}Sb_{1.5}Te_3$/PEDOT:PSS composite, by coating $Bi_{0.5}Sb_{1.5}Te_3$ fillers with highly conductive CuTe layer. With highly crystallized PEDOT:PSS prepared as the matrix, high-performance Cu-$Bi_{0.5}Sb_{1.5}Te_3$ /PEDOT:PSS film is fabricated with promising $\sigma$ of ~2300 S $cm^{-1}$ and peak $S^2\sigma$ of 312 μW $m^{-1}$ $K^{-2}$ at room temperature, which reaches to a record-high value in the reported $Bi_{0.5}Sb_{1.5}Te_3$/PEDOT:PSS composites. Accordingly, a home-made flexible thermoelectric device is fabricated using our prepared composites, generating a promising open-circuit thermovoltage of ~7.7 mV with the human wrist as the thermal source. This study addresses the significance of interfacial carrier transport, hinting the bright prospects of cheap conductive polymers as the effective power source of wearable electronics.

***Keywords***: Thermoelectrics, Flexible, PEDOT:PSS, Bismuth telluride, Interface

## 1. Introduction

Rapid advances of the Internet of Things (IoT) spark the increasing developments of miniature and integrated wearable electronics, where conventional batteries as the power source have severe disadvantages such as frequent replacements/recharge and extra maintenance.[1, 2] Flexible thermoelectric (FTE) materials enable the direct power generation from heat through the Seebeck effect and can present conformal interactions with heat sources to maximize heat harvesting, which can, therefore, act as energy-autonomous, maintenance-free and emission-free power sources for wearable electronics.[3] To evaluate the power generation efficiency of FTE materials, a dimensionless figure of merit ($zT$) is defined as: $zT = S^2\sigma T/\kappa$, where $S$, $\sigma$, $\kappa$, and $T$ is the Seebeck coefficient, electrical conductivity, thermal conductivity, and operating temperature, respectively.[4] Promising $zT$ can thus be effectively contributed by high power factor ($S^2\sigma$) and low $\kappa$. Currently, studies on FTE materials mainly focus on conductive polymers, such as poly(3,4-ethylenedioxythiophene)-poly(styrenesulfonate) (PEDOT:PSS),[5-8] poly(3-hexylthiophene-2,5-diyl) (P3HT),[9-11] and polyaniline (PANI),[12-16] due to their intrinsic flexibility and low $\kappa$. However, their poor electrical properties result in inferior $S^2\sigma$ than inorganic TE materials, which restricts their $zT$ improvements. In this regard, optimizing the electrical properties of conductive polymers is of vital significance.

So far, several strategies have been used to increase $S^2\sigma$ of conductive polymers. For example, improved $\sigma$ of PEDOT:PSS can be realized from ordered microstructure or improved crystallinity after polar solvents pre-treatments with dimethyl sulfoxide (DMSO)[17, 18] or ethylene glycol (EG),[19-21] or concentrated $H_2SO_4$ post-treatments.[8, 22] $S$ can be effectively tuned with controlled oxidation levels of conductive polymers, by means of reducing PEDOT-Tos film in the

tetrakis(dimethylamino)ethylene (TDAE) atmosphere,[23] or immersing PEDOT:PSS film in reducing $NaBH_4$,[24] NaOH[5] and $N_2H_4$[24] solutions.

Additionally, incorporating inorganic TE fillers into conductive polymers matrix has also been proposed to be an effective strategy to boost $S^2\sigma$,[25-29] where FTE composites might be synergistically endowed with decent $S^2\sigma$ of inorganic TE fillers and low $\kappa$ of conductive polymers. So far, FTE composites mainly focus on PEDOT:PSS as the polymer matrix, due to its promising $\sigma$ of 4380 S $cm^{-1}$ at room temperature,[22] abundance, and facile processability, which may be beneficial for scale-up productions. Inorganic TE fillers mainly include $Bi_2Te_3$[26, 29, 30] and $Bi_{0.5}Sb_{1.5}Te_3$ (BST)[25] considering their decent low-temperature $S^2\sigma$, or Te[27, 31, 32] and SnSe[33] due to their outstanding low-temperature $S$. Effectively enhanced $S^2\sigma$ of 32.26 μW $m^{-1}$ $K^{-1}$ has been witnessed from BST/PEDOT:PSS composite, which presents more than three times higher value than pristine PEDOT:PSS film.[25] In spite of the progress, $S^2\sigma$ of FTE composite is still much inferior to inorganic TE materials, possibly caused by the overlook of interfacial carrier transports between fillers and polymers, which significantly restrains contributions of fillers to $S^2\sigma$. By applying surface engineering to inorganic fillers, interfacial carrier transports can be optimized, and in turn, further boost of $S^2\sigma$ becomes possible.[26, 30] Typically, Zhang *et al.*[26] applied HCl rinsing to remove the potential oxidation layer on the surface of *p*-type $Bi_2Te_3$ filler to optimize interfacial carrier transports, and found significantly increased $S^2\sigma$ of 131 μW $m^{-1}$ $K^{-1}$ in the $Bi_2Te_3$/PEDOT:PSS film, compared with that of 35.6 μW $m^{-1}$ $K^{-1}$ without HCl rinsing. Recently, Goo *et al.*[30] conducted proton-irradiation treatments on the surface of $Bi_2Te_3$ fillers, which intentionally induced surface defect sites as the extra adsorption sites for polymer chains, and in turn led to intensified interfacial interactions. Consequently, an outstanding $S^2\sigma$ of 325.3 μW $m^{-1}$ $K^{-1}$ was achieved in the $Bi_2Te_3$/PEDOT:PSS film,[30] which is among the top values of

$Bi_2Te_3$/PEDOT:PSS composites. Therefore, surface engineering of fillers is a promising approach in securing splendid $S^2\sigma$ in FTE composites.

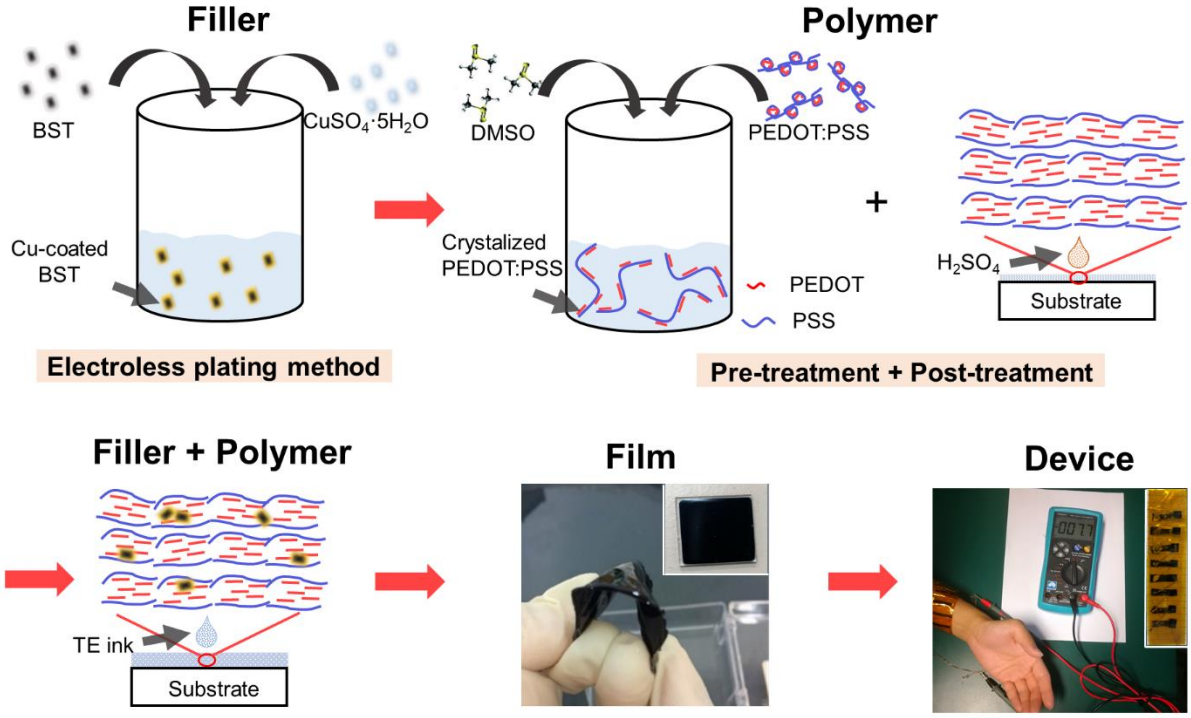


**Fig. 1.** Schematic illustration of the processes to fabrication Cu-BST/PEDOT:PSS FTE films and device.

In this study, we develop a new strategy to optimize interfacial carrier transports in the BST/PEDOT:PSS composite, by coating BST fillers with highly conductive CuTe layer ($\sigma$>5.2×10$^5$ S cm$^{-1}$).[34] With highly crystallized PEDOT:PSS prepared as the matrix, superhigh-performance Cu-BST/PEDOT:PSS film was fabricated and showed promising $\sigma$ of 2270 S cm$^{-1}$ and peak $S^2\sigma$ of 312 μW m$^{-1}$ K$^{-1}$ at room temperature, which reached to state-of-the-art values reported for BST/PEDOT:PSS composites.[25, 26, 35, 36] **Fig. 1** schematically depicts the fabrication process of the composites, where fillers and polymers are separately prepared. Cu-BST fillers were synthesized by a facile electroless plating method.[37, 38] Crystallized PEDOT:PSS was obtained

through DMSO polar solvent pre-treatments, followed by concentrated $H_2SO_4$ post-treatment to selectively remove insulating PSS, which in turn render increased $\sigma$. Finally, the BST/PEDOT:PSS film with decent flexibility was fabricated by drop-casting TE ink onto a pre-cleaned glass substrate. A home-made FTE device was fabricated accordingly, showing the effective power generation with the human wrist as the thermal source.

## 2. Experimental section

### *2.1 Materials*

Analytical grade Bi shots (99.999%), Sb shots (99.999%), Te shots (99.999%) and NaOH (99.999%) were purchased from Alfa-Aesar (United States) and used without any further purifications. PEDOT:PSS aqueous solution (Clevios PH1000) was purchased from Heraeus (Germany). Dimethyl sulfoxide (DMSO), concentrated $H_2SO_4$ (98%), concentrated $HNO_3$ (98%), copper sulfate pentahydrate, formaldehyde, Ethylenediaminetetraacetic acid disodium salt (EDTA-2Na) and polyvinylidene difluoride (PVDF) membrane filter (0.45 μm pore size) were all purchased from Sigma-Aldrich (Australia).

### *2.2 Synthesis of Cu-coated BST fillers*

High-purity Bi shots (99.999%), Sb shots (99.999%) and Te shots (99.999%) were weighted based on the nominal composition of BST, and subsequently sealed into a quartz tube under the vacuum of $10^{-3}$ Pa. The quartz tube was then placed in the furnace, where the precursors were melted and kept for 10 h at 1023 K. As-synthesized BST ingot was finally ball-milled (AXT, 8000M) for 20 min under 15 Hz in order to obtain fine BST fillers.

As-prepared BST fillers were then coated with Cu using facile electroless plating method. Specifically, BST fillers were firstly sonicated in 5% $HNO_3$ solution for 1 h, followed by deionized water rinsing for at least three times to remove residual impurities. Afterwards, pretreated BST

fillers were transferred into the coating solution consisting of copper sulfate pentahydrate as the copper source, formaldehyde as the reducing agent, EDTA-2Na as the complex agents and NaOH to provide the alkaline environment. The coating process was conducted under the sonication and lasted for 1 h at 330 K. The as-coated BST fillers were alternatively washed by deionized water and ethonal for at least three times, before being collected by centrifugation and dried at 330 K in the oven overnight. The as-collected Cu-BST fillers were ultimately reduced under $H_2$ atmosphere at 580 K for 1 h, and naturally cooled down to the room temperature. The as-reduced Cu-BST fillers were sealed in the vacuum and ready for the next step.

*2.3 Treatments of PEDOT:PSS conductive polymers*

Aqueous solution PEDOT:PSS was firstly mixed with 10 *vol*.% polar solvent DMSO and sonicated for 6 h at 330 K. The solution was then filtered by PVDF membrane (0.45 μm pore size) using vacuum-assisted filtration method to remove insulating and hydrophilic PSS. The filtrate was collected and magnetically stirred until forming the PEDOT:PSS slurry, which was subsequently drop casted onto pre-cleaned silicon dioxide substrates, and later dried at 330 K for 20 min on the heating plate. PEDOT:PSS films were then immersed into concentrated $H_2SO_4$ (98%) for 10 h to further remove insulating PSS, and rinsed with deionized water for three times afterwards. The as-treated PEDOT:PSS films were lastly magnetically stirred into PEDOT:PSS slurry, which was ready for the film fabrication.

*2.4 Fabrication of Cu-BST/PEDOT:PSS films*

Silicon dioxide substrates were pre-cleaned following the sequence of detergent, deionized water, ethanol and plasma cleaning. PEDOT:PSS slurry was mixed with different amount of Cu-BST fillers (2 *wt*.%, 4 *wt*.% and 6 *wt*.%) and sonicated for 6 h, followed by intense magnetic stirring for another 6 h at room temperature to obtain uniform Cu-BST/PEDOT:PSS inks. BST fillers

without Cu coating were also mixed with PEDOT:PSS slurry following above processes as the contrast set. 100 μL ink was subsequently drop casted onto pre-cleaned silicon dioxide substrates, and later dried at 330 K for 20 min on the heating plate. The as-fabricated films were collected and showed decent flexibility.

*2.5 Fabrication of FTE device*

10 milliliters of as-prepared inks was paved in the glass petri dish with the diameter of 55 mm. After drying at 330 K for 2 hours, as-fabricated film was immersed in ethanol to detach from the glass petri dish. Free-standing Cu-BST/PEDOT:PSS films were obtained by collecting detached film and drying at 330 K for 20 min. As-obtained films were cut into rectangular pieces with the size of 25 × 8 $mm^2$, which were subsequently connected by copper wires and assembled into FTE device using polyimide as the substrate Two polyimide films were lastly used to cover top and bottom of the FTE device, acting as the protection layer.

*2.6 Measurements and characterization*

Electrical properties of as-fabricated films, including $\sigma$ and $S$, were measured by SBA458 (Netzsch) at 300 K. X-ray diffraction (XRD, Bruker-D8) was applied to determine the crystal structure of BST fillers before and after Cu coatings. Grazing incidence XRD (GIXRD, Rigaku SmartLab) was utilized to investigate the crystallinity of conductive polymers before and after treatments. Scanning electron microscopy (SEM, JEOL JSM-7100F) and transmission electron microscopy (TEM, TECNAI-F20) were utilized to study the morphology and structural characteristics. X-ray energy-dispersive spectroscopy (EDS) mapping and spot analysis (equipped in HITACHI-SU3500 SEM) were conducted to confirm the successful surface coating of Cu on the BST fillers.

**3. Results and discussion**

**Fig. 2** shows the structural characterizations of BST fillers before and after Cu coating. **Fig. 2a** is XRD patterns taken from BST, 0.05 *wt*.% Cu-BST and 0.1 *wt*.% Cu-BST fillers, respectively. As can be seen, the diffraction peaks of the as-synthesized BST powders can be exclusively indexed as hexagonal structured BST with lattice parameters of $a$ = 4.28424 nm and $c$ = 30.52389 nm and a space group of $R\bar{3}$m (PDF#49-1713). After Cu coating, additional peaks at $2\theta$ of $12.8^0$, $25.4^0$ and $31.1^0$ emerge in the diffraction peaks of 0.05 *wt*.% Cu-BST, which can be precisely retrieved as orthorhombic structured CuTe with lattice parameters of $a$ = 3.16 nm, b = 4.08 nm and $c$ = 6.93 nm and a space group *P*mmn (PDF#22-0252). This indicates that Cu reacts with BST particles during the coating process to form CuTe. **Fig. 2b** shows the EDS results, and further confirms the successful coating of Cu on the surface of BST particles, where Cu is detected from EDS spot analysis and clearly observed on the boundaries of BST particles from the EDS maps. **Fig. 2c-g** are TEM results to clarify the insights of the coating process. As can be seen, the uncoated BST particles (**Fig. 2c**) show relatively smooth boundaries, while zig-zag boundaries appear in the coated BST particles (**Fig. 2d**), which is attributed to the $HNO_3$ pre-treatments to generate sufficient reaction sites for maximum Cu coating. As verified in **Fig. 2d** and **e,** CuTe is clearly observed on BST boundaries, which is consistent with SEM EDS maps, shown in **Fig. 2b**. **Fig. 2e** shows typical high-resolution TEM image, in which the as-coated CuTe layer is relatively uniform with a thickness of 17 nm. **Fig. 2f** is its corresponding high-angle annular dark-field (HAADF) image of the interface, where the CuTe layer with small atomic mass shows dark contrast compared with the bright contrast of the BST particle. **Fig. 2g** is a zoom-in high-resolution TEM (HRTEM) image taken from the CuTe layer (highlighted by red square in **Fig. 2e**), in which two sets of lattice planes with $d$-spacing of 0.18 and 0.23 nm can be detected with the angle of $50.3^0$ that correspond to the (022) and (102) atomic planes of CuTe, respectively.

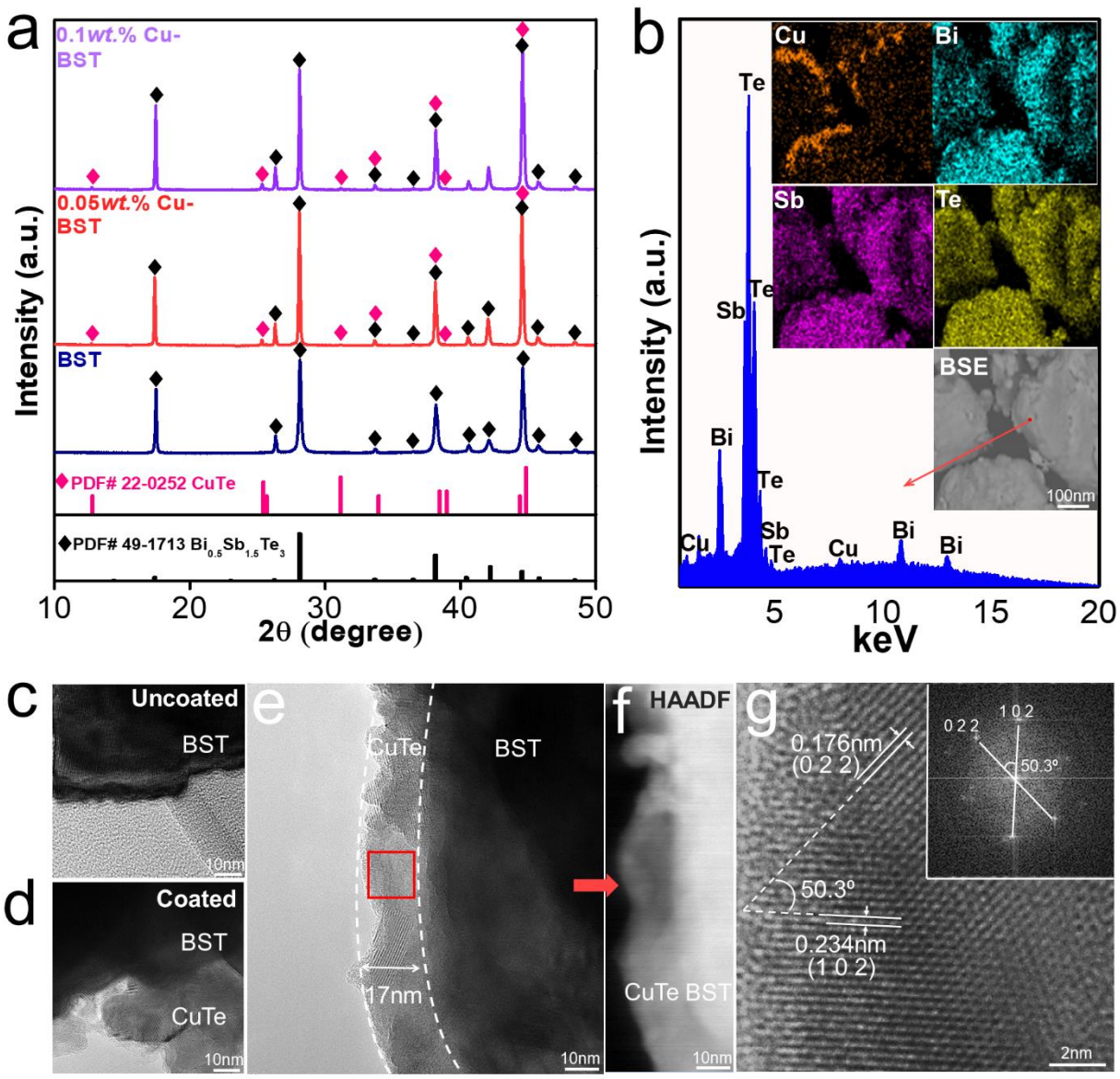


**Fig. 2.** (a) XRD patterns of BST, 0.05 *wt*.% Cu-BST and 0.1 *wt*.% Cu-BST fillers. (b) EDS spot spectrum of 0.1 *wt*.% Cu-BST fillers with the inset of mappings of Cu, Bi, Sb and Te. Typical high-magnitude TEM images of BST fillers (c) before and (d) (e) after Cu coating, together with corresponding (f) HAADF and (g) HRTEM images.

It has been reported that high crystallinity of PEDOT:PSS can lead to high $\sigma$,[22] while selectively removal of insulating PSS can induce improved crystallinity of PEDOT:PSS.[39] Here, we applied

DMSO-$H_2SO_4$ double treatments to effectively remove insulating PSS and in turn result in highly crystallized PEDOT:PSS. **Fig. 3a** shows XRD patterns of PEDOT:PSS films before and after the treatments. The pristine film shows weak peaks at low $2\theta$ of 3.3 and $7^o$ corresponding to the lamella stacking of alternate PEDOT and PSS along the (100) plane, and high $2\theta$ of 18 and $26^0$, which can be attributed to amorphous PSS and inter-chain planar stacking along the (010) planes.[40] The weak intensities of all diffraction peaks indicate the amorphous microstructure and low crystallinity of pristine PEDOT:PSS film. These form a sharp contrast with DMSO-$H_2SO_4$ treated PEDOT:PSS film, where two sharp diffraction peaks at ~7 and $12.5^0$ indicate that (100) stacking has been greatly intensified after the treatment. Moreover, it should be noted that two peaks of (100) stacking both exhibit an obvious right peak shift after the treatment, which is from the original $2\theta$ of 3.3 and $7^0$ to ~7 and $12.5^0$, respectively. According to Bragg's law,[8] this hints the shrink of spacing between (100) stackings, which confirms the effective removal of insulating PSS. On the other hand, two peaks of (010) planes stacking are still quite weak after the treatment, and present ignorable intensities compared with two peaks of (010) stacking. This means (100) stacking dominates in the microstructure of treated film, which contributes to highly crystallized PEDOT:PSS. Increased crystallinity of PEDOT:PSS is also associated with chemical structure transition of PEDOT monomers from benzoid to quinoid after DMSO-$H_2SO_4$ double treatments,[41, 42] as shown in **Fig. 3a**. PEDOT monomers with benzoid structure are connected by relatively flexible C-C bonds, which tend to induce deviations of adjacent thiophene rings and formation of coiled-up conformation.[43] However, PEDOT monomers with quinoid structure are connected by rigid π bonds (C=C bonds), which is favored by flat PEDOT backbones and in turn enhanced crystallinity.[42] Cross-sectional SEM images of PEDOT:PSS films of **Fig. 3b** further confirm the

improved crystallinity, where lamella stacking is clearly visible after the treatment. Additionally, the decreased thickness of film from 4 to 2.5 μm verifies the PSS depletion.

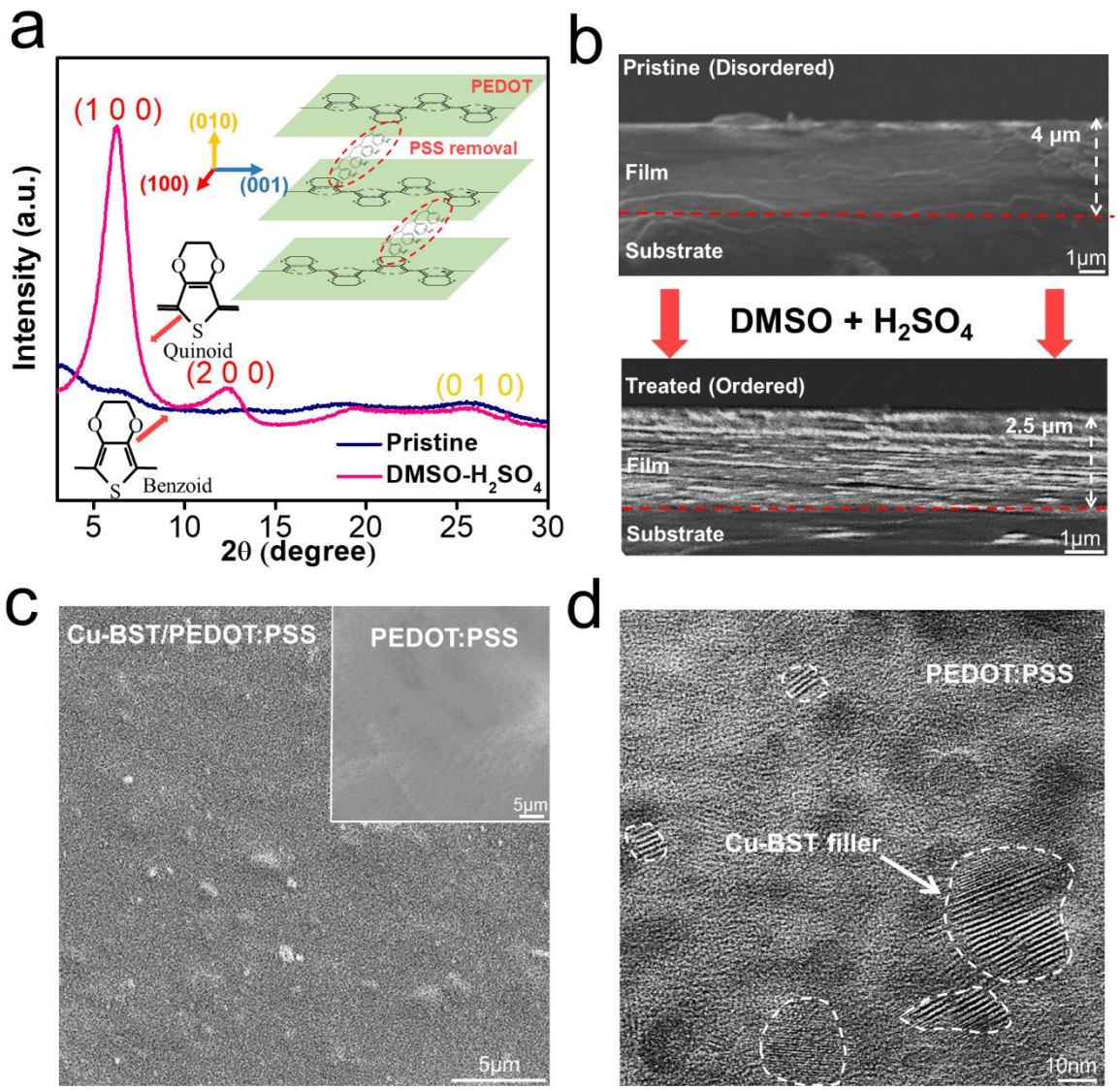


**Fig. 3.** (a) XRD patterns and (b) cross-sectional SEM images of PEDOT:PSS films before and after DMSO-$H_2SO_4$ double treatments. (c) Typical top-view SEM and (d) TEM images of PEDOT:PSS films with 6 *wt*.% Cu-BST filler incorporation, with the inset of (c) showing PEDOT:PSS film without fillers.

With Cu-coated BST fillers and crystallized PEDOT:PSS conductive polymer, Cu-BST/PEDOT:PSS film was fabricated. **Fig. 3c** shows the typical top-view SEM image of the film, with the inset of PEDOT:PSS film without fillers. Relatively uniform dispersion of fillers can be observed, and the introduction of fillers results in the improved roughness of the films. **Fig. 3d** is a TEM image, and further confirms the well dispersion of fillers. It should be noted that the size of fillers in our study are typically ~400 nm, as shown in **Fig. S2**. The smaller filler size observed in **Fig. 3d** can be attributed to blocking effects of conductive polymers towards TEM electron beams, where partial lattice structures of inorganic fillers underneath conductive polymers cannot be observed. Moreover, PEDOT:PSS is observed to closely envelop Cu-BST fillers, which can be beneficial to optimize the interfacial carrier transport.

**Fig. 4** plots the room-temperature $\sigma$ and $S$ of the as-fabricated films. **Fig. 4a** shows DMSO-$H_2SO_4$ treated PEDOT:PSS films, in which decent $\sigma$ of 1815 S cm$^{-1}$ is achieved, which is ascribed to the as-obtained high crystallinity. This value agrees with reported crystalline PEDOT:PSS.[8, 22] With filler incorporations, it is found that pristine BST fillers can deteriorate $\sigma$, showing values lower than treated PEDOT:PSS films. On one hand, this may be due to the lower $\sigma$ value of pristine BST fillers (~ 500 S cm$^{-1}$, **Fig. S1a**) than treated PEDOT:PSS. On the other hand, the surface of pristine BST fillers can potentially scatter carriers during the transport due to the relatively high interfacial contact resistance, which leads to the depressed carrier mobility ($\mu$) and in turn low $\sigma$.

With introducing highly conductive CuTe interfacial layers, $\sigma$ can be significantly enhanced and exceed that of treated PEDOT:PSS films under various filler contents. Such a tendency is more obvious with increasing the Cu coating, and an outstanding $\sigma$ value of 2520 S cm$^{-1}$ is achieved in the 0.1 *wt*.% Cu-BST/PEDOT:PSS film with 2 *wt*.% filler content. Such a $\sigma$ improvement can be attributed to high $\sigma$ value of the CuTe layers ($\sigma$>5.2×10$^5$ S cm$^{-1}$),[34] as well as the optimized

interfacial carriers transport, as schematically depicted in **Fig. 4b**. In contrast to the carrier blocking effect induced by pristine BST fillers, highly conductive CuTe interfacial layers can render carriers to travel through BST fillers, rather than being scattered. In this way, optimized interfacial carriers transport with improved $\mu$ is generated, which is favorable by high $\sigma$. To manifest above claims, series- and parallel-connection models are employed to predict $\sigma$ and $S$ of hybrid films with 4*wt*. % filler content and compare with our experimental results. The results are illustrated in **Fig. S3**. Without Cu coating, both $\sigma$ and $S$ lie beyond the prediction range. This can be understood as that most carriers are scattered at the interface, deteriorating system electrical properties. After Cu coating, the system shows reasonable results within the prediction range, which indicates the "blocking" effects of fillers are mitigated due to reduced interfacial contact resistance. This contrast supports our claims of optimized interfacial transport.

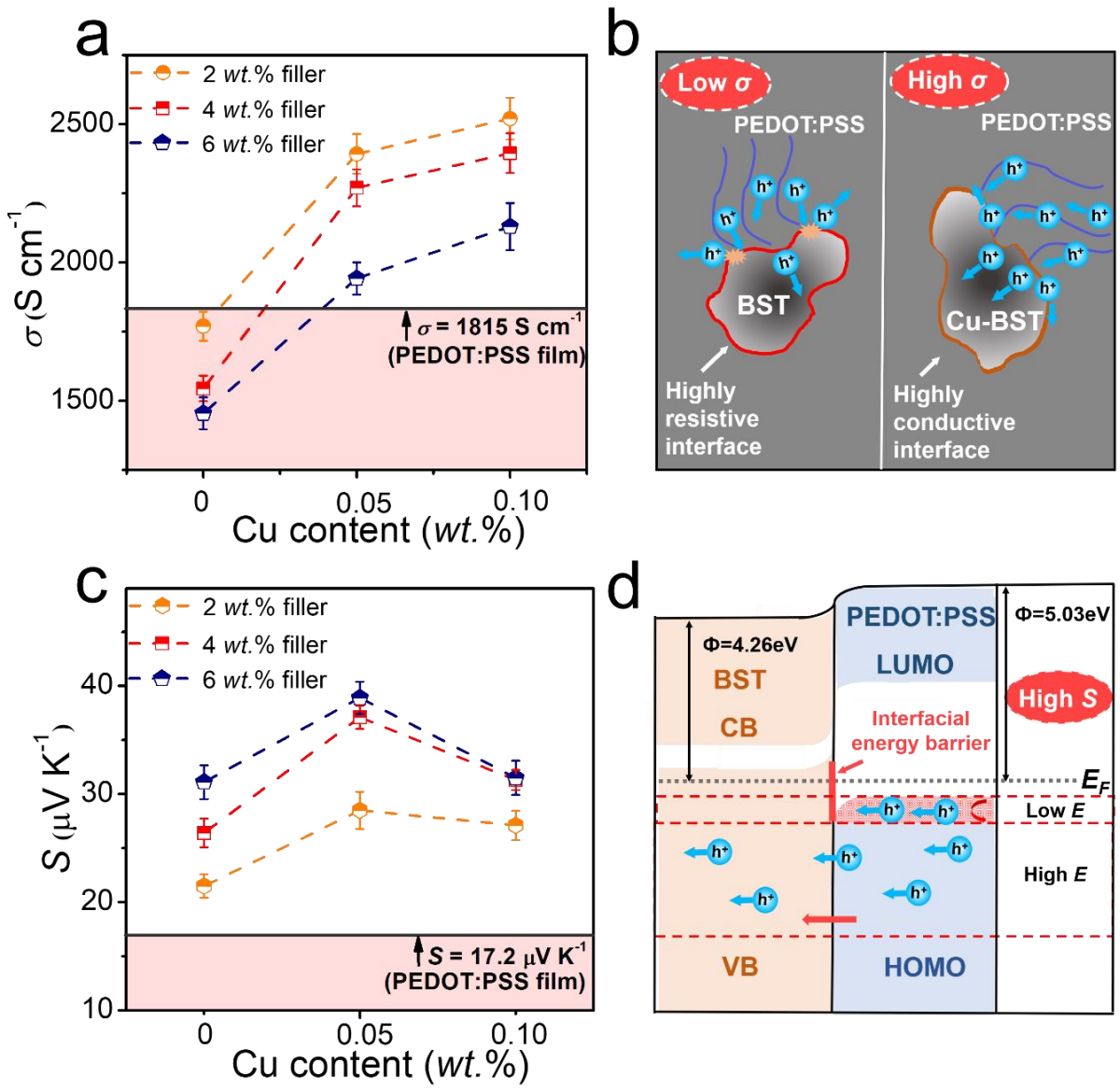


**Fig. 4.** Measured room-temperature (a) $\sigma$ and (c) $S$ of PEDOT:PSS films incorporated with BST fillers before and after Cu coatings (filler content 2 *wt*.%, 4 *wt*.% and 6 *wt*.%), with corresponding schematics of (b) optimized interfacial carrier transports and (d) interfacial energy filtering.

**Table 1**. ***n*** **and** ***μ*** **of BST/PEDOT:PSS films before and after Cu coatings (4** ***wt*****.% filler).**

| Parameter | BST/PEDOT:PSS | 0.05 *wt*.% Cu-BST/PEDOT:PSS | 0.1 *wt*.% Cu-BST/PEDOT:PSS |
|---|---|---|---|
| $\mu$ ($cm^2\ V^{-1}\ s^{-1}$) | 13.72±1.96 | 18.04±2.21 | 18.82±2.82 |
| $n$ ($10^{20}\ cm^{-3}$) | 8.06±1.21 | 8.29±1.24 | 8.37±1.19 |

Hall measurements are applied to investigate the change of carrier concentration ($n$) and $\mu$ before and after Cu coatings, and **Table 1** summarizes the results. $n$ is observed to improve from ~8.06 to ~8.28 and ~8.37 × $10^{20}$ $cm^{-3}$ after Cu coatings, which is caused by the introduction of Cu, as manifested by $n$ of BST before and after Cu coatings in **Fig. S1c**. Effective increased $\mu$ occurs from ~13.72 to ~18.04 and ~18.82 $cm^2$ $V^{-1}$ $s^{-1}$ after Cu coatings. This verifies the optimization of interfacial carrier transports and accounts for increased $\sigma$. Additionally, high filler contents are found to cause low $\sigma$. This agrees with other reports,[44, 45] and stems from more introduced interfaces between polymers and fillers.

In terms of $S$, **Fig. 4c** shows that additions of fillers before and after Cu coatings both show positive effects. Peak $S$ of 38.9 μV $K^{-1}$ can be achieved from 0.05 *wt*.% Cu-BST/PEDOT:PSS films with 6 *wt*.% filler content. The $S$ improvement is contributed by the interfacial energy filtering effect,[46, 47] as shown in **Fig. 4d**. With the interfacial energy offset existing between PEDOT:PSS and BST fillers, an interfacial energy barrier can be formed between the highest occupied molecular orbital (HOMO) of PEDOT:PSS and valance band (VB) of BST fillers. Carriers (holes) with relatively low energy tend to be scattered at the interfaces while those with high energy pass through. Therefore, the average energy of system carriers is improved, which is favored by high $S$.[47] On the other hand, it should be noted that Cu-BST fillers (both 0.05 *wt*.% and 0.1 *wt*.%) possess boosted $S$ compared with BST fillers. This may because introduced CuTe layers reduce interfacial contact resistance, allowing more carriers to transport through BST fillers to induce more sufficient interfacial energy filtering. With increasing the amount of Cu coating, $S$ of Cu-BST fillers reduces due to increased $n$, as shown in **Fig. S1b** and **c**, which consequently leads to slightly dropped $S$.

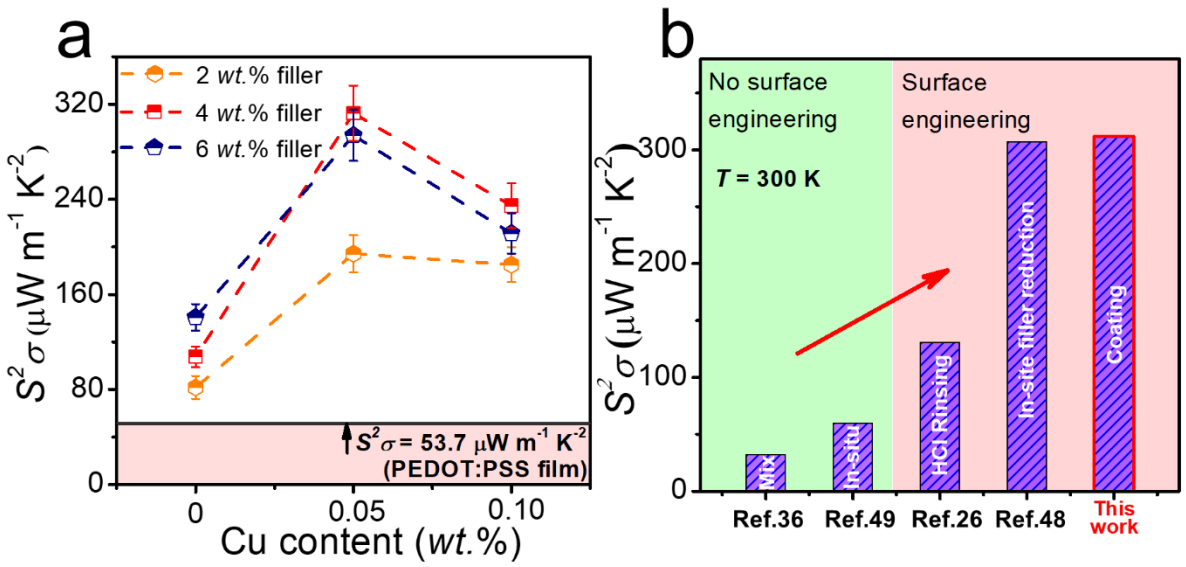


**Fig. 5.** (a) Measured room-temperature $S^2\sigma$ of PEDOT:PSS films incorporated with BST fillers before and after Cu coatings (filler content 2 *wt*.%, 4 *wt*.% and 6 *wt*.%). (b) Comparisons of $S^2\sigma$ between this work and other reported BST/PEDOT:PSS works,[26, 36, 48, 49] where the potentials of filler surface engineering are visible.

With the measured $\sigma$ and $S$, $S^2\sigma$ is calculated and plotted in **Fig. 5a**. The $S^2\sigma$ enhancement induced by Cu coating is evident, and an outstanding $S^2\sigma$ value of 312 μW m$^{-1}$ K$^{-2}$ can be observed in the 0.05 *wt*.% Cu-BST/PEDOT:PSS film with 4 *wt*.% filler content, which exhibits almost six times improvements than our treated PEDOT:PSS film. Compared with other BST/PEDOT:PSS FTE works,[26, 36, 48, 49] **Fig. 5b** shows the outstanding performance of our strategy, in which significant $S^2\sigma$ enhancement is obtained after considerations of interfaces, manifesting surface engineering of fillers.

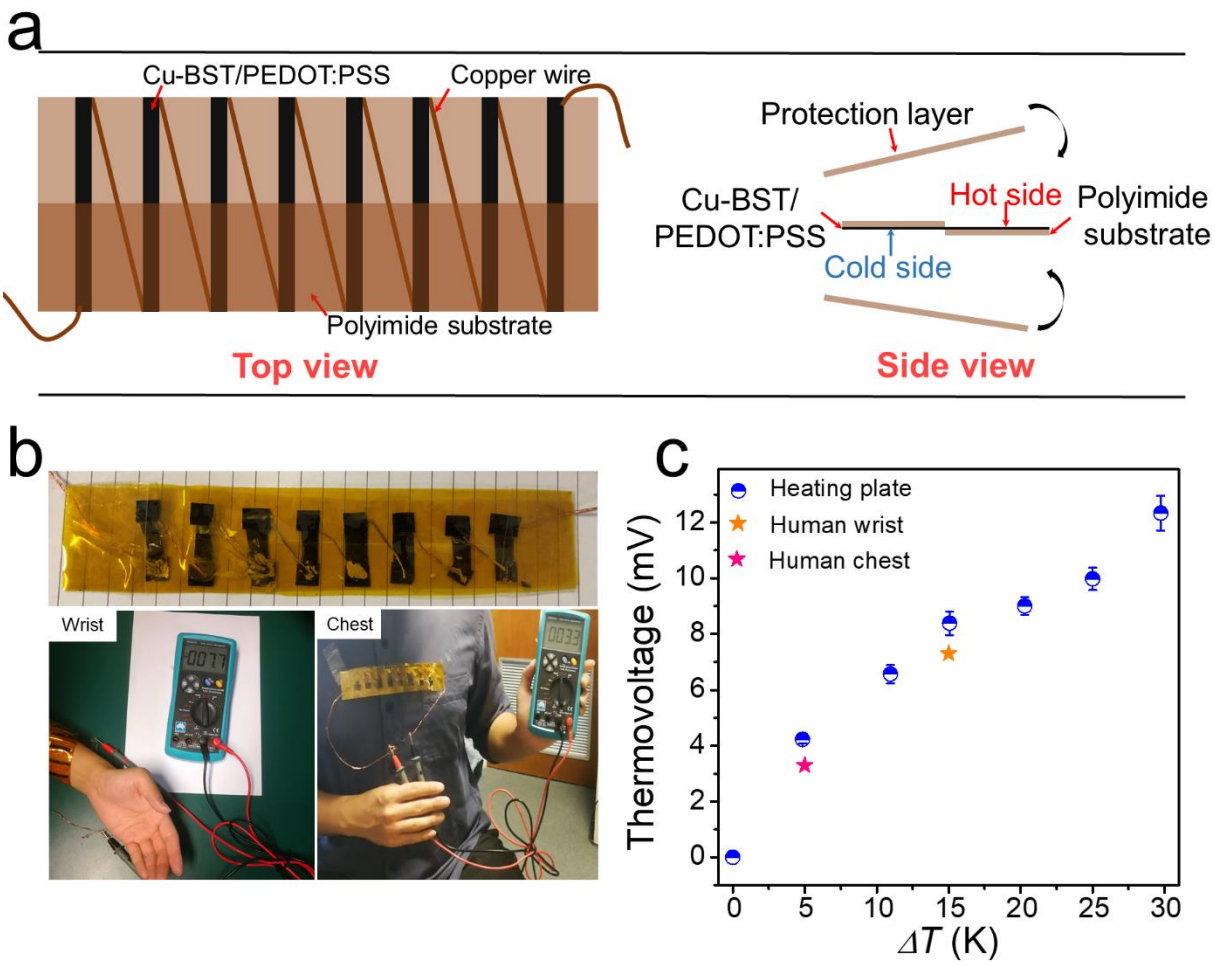


**Fig. 6.** (a) Schematic diagram of a home-made FTE device. (b) Images of the as-fabricated FTE device, and its thermovoltage generations with human wrist and chest as thermal sources. (c) Measured thermovoltages using heating plate, human wrist and chest as thermal sources.

To confirm the potentials of power generation using the as-prepared Cu-BST/PEDOT:PSS films, a home-made FTE device was fabricated based on the structure shown in **Fig. 6a**. TE legs with the size of 25 × 8 $mm^2$ were assembled into the flexible polyimide substrate and connected by copper wires. Another two polyimide films were applied as the protection layer to cover top and bottom of TE legs. **Fig. 6b** shows the as-fabricated FTE device, where thermovoltages can be effectively generated when attaching the device onto human wrist and chest.[50-54] By firmly attaching one end

of the device onto the heating plate and exposing the other end in the air, more temperature differences can be achieved from 5 to 30 K, generating increased thermovoltages, as shown in **Fig. 6c**. Peak thermovoltage of ~12.3 mV can be realized with 30 K temperature difference between two ends of the device. It should be noted that heating plate as the thermal source can contribute slightly higher voltages than human body. This should be due to the heat loss occurred at the interface between human skin and the device, leading to reduced temperature differences and in turn deteriorated voltage generations.

## 4. Conclusions

In summary, we fabricated superhigh-performance Cu-BST/PEDOT:PSS FTE films by coating BST fillers with a highly conductive CuTe layer ($\sigma$>5.2×10$^5$ S cm$^{-1}$) and preparing highly crystallized PEDOT:PSS conductive polymer. High $\sigma$ of 2270 S cm$^{-1}$ was achieved, which is attributed to the boosted interfacial carriers transport and crystallized PEDOT:PSS. Meanwhile, $S$ was enhanced by interfacial energy filtering, reaching value up to 37.1 μV K$^{-1}$. Systematic XRD, EDS, SEM and TEM results confirm the successful introduction of nanoscale CuTe layers and the accomplishment of highly crystallized PEDOT:PSS. Effectively improved $\sigma$ of the system after Cu coating manifests the optimization of interfacial carriers transport, which is further supported by Hall measurement results. As a result, an outstanding $S^2\sigma$ value of 312 μW m$^{-1}$ K$^{-2}$ was realized at the room temperature, which serves as a state-of-the-art value for BST/PEDOT:PSS FTE composites. Meanwhile, a FTE device was fabricated using the as-prepared Cu-BST/PEDOT:PSS films, generating a promising open-circuit thermovoltage of ~7.7 mV with the human wrist as the thermal source.

## Notes

The authors declare no competing financial interest.

**Acknowledgements**

This work was financially supported by the Australian Research Council. ZGC thanks the USQ start-up grant and strategic research grant. Microscopy Australia is acknowledged for providing characterization facilities.

**Supporting Information**

Supporting information of this article can be found online free of charge.

**References**

[1] Y. Wang, L. Yang, X. L. Shi, X. Shi, L. Chen, M. S. Dargusch, J. Zou, Z. G. Chen, Flexible thermoelectric materials and generators: challenges and innovations, Adv. Mater. 31 (2019) e1807916.

[2] B. Russ, A. Glaudell, J. J. Urban, M. L. Chabinyc, R. A. Segalman, Organic thermoelectric materials for energy harvesting and temperature control, Nat. Rev. Mater. 1 (2016) 16050.

[3] Y. Ding, Y. Qiu, K. Cai, Q. Yao, S. Chen, L. Chen, J. He, High performance n-type Ag2Se film on nylon membrane for flexible thermoelectric power generator, Nat. Commun. 10 (2019) 841.

[4] Z. G. Chen, G. Han, L. Yang, L. Cheng, J. Zou, Nanostructured thermoelectric Materials: Current Research and Future Challenge, Prog. Nat. Sci. 22 (2012) 535-549.

[5] Z. Fan, P. Li, D. Du, J. Ouyang, Significantly enhanced thermoelectric properties of PEDOT:PSS films through sequential post-treatments with common acids and bases, Adv. Energy Mater. 7 (2017) 1602116.

[6] N. Kim, S. Kee, S. H. Lee, B. H. Lee, Y. H. Kahng, Y.-R. Jo, B.-J. Kim, K. Lee, Highly conductive PEDOT:PSS nanofibrils induced by solution-processed crystallization, Adv. Mater. 26 (2014) 2268-2272.

[7] Q. Wei, M. Mukaida, Y. Naitoh, T. Ishida, Morphological change and mobility enhancement in PEDOT:PSS by adding co-solvents, Adv. Mater. 25 (2013) 2831-2836.

[8] S. Xu, M. Hong, X. L. Shi, Y. Wang, L. Ge, Y. Bai, L. Wang, M. Dargusch, J. Zou, Z. G. Chen, High-performance PEDOT:PSS flexible thermoelectric materials and their devices by triple post-treatments, *Chem. Mater.* 31 (2019) 5238-5244.

[9] Q. Zhang, Y. Sun, W. Xu, D. Zhu, Thermoelectric energy from flexible P3HT films doped with a ferric salt of triflimide anions, Energy Environ. Sci. 5 (2012) 9639-9644.

[10] L. Chen, W. Liu, Y. Yan, X. Su, S. Xiao, X. Lu, C. Uher, X. Tang, Fine-tuning the solid-state ordering and thermoelectric performance of regioregular P3HT analogues by sequential oxygen-substitution of carbon atoms along the alkyl side chains, *J. Mater. Chem. C* 7 (2019) 2333-2344.

[11] S. Qu, Q. Yao, L. Wang, Z. Chen, K. Xu, H. Zeng, W. Shi, T. Zhang, C. Uher, L. Chen, Highly anisotropic P3HT films with enhanced thermoelectric performance *via* organic small molecule epitaxy, NPG Asia Mater. 8 (2016) e292.

[12] Q. Yao, L. Chen, W. Zhang, S. Liufu, X. Chen, Enhanced thermoelectric performance of single-walled carbon nanotubes/polyaniline hybrid nanocomposites, ACS Nano 4 (2010) 2445-2451.

[13] H. Zengin, W. Zhou, J. Jin, R. Czerw, D. W. Smith Jr., L. Echegoyen, D. L. Carroll, S. H. Foulger, J. Ballato, Carbon nanotube doped polyaniline, Adv. Mater. 14 (2002) 1480-1483.

[14] Q. Yao, Q. Wang, L. Wang, L. Chen, Abnormally enhanced thermoelectric transport properties of SWNT/PANI hybrid films by the strengthened PANI molecular ordering, Energy Environ. Sci. 7 (2014) 3801-3807.

[15] Q. Yao, Q. Wang, L. Wang, Y. Wang, J. Sun, H. Zeng, Z. Jin, X. Huang, L. Chen, The synergic regulation of conductivity and Seebeck coefficient in pure polyaniline by chemically changing the ordered degree of molecular chains, J. Mater. Chem. A 2 (2014) 2634-2640.

[16] K. Lee, S. Cho, S. Heum Park, A. J. Heeger, C.-W. Lee, S. H. Lee, Metallic transport in polyaniline, Nature 441 (2006) 65-68.

[17] J. Ouyang, C.-W. Chu, F. C. Chen, Q. Xu, Y. Yang, High-conductivity poly(3,4-ethylenedioxythiophene):poly(styrene sulfonate) film and its application in polymer optoelectronic devices, Adv. Funct. Mater. 15 (2005) 203-208.

[18] Y. Xia, J. Ouyang, PEDOT:PSS films with significantly enhanced conductivities induced by preferential solvation with cosolvents and their application in polymer photovoltaic cells, J. Mater. Chem. 21 (2011) 4927-4936.

[19] G. H. Kim, L. Shao, K. Zhang, K. P. Pipe, Engineered doping of organic semiconductors for enhanced thermoelectric efficiency, Nat. Mater. 12 (2013) 719-723.

[20] J. Ouyang, Q. F. Xu, C. W. Chu, Y. Yang, G. Li, J. Shinar, On the mechanism of conductivity enhancement in poly (3,4-ethylenedioxythiophene): poly(styrene sulfonate) film through solvent treatment, Polymer 45 (2004) 8443-8450.

[21] J. Y. Kim, J. H. Jung, D. E. Lee, J. Joo, Enhancement of electrical conductivity of poly(3,4-ethylenedioxythiophene)/poly(4-styrenesulfonate) by a change of solvents, Synth. Metals 126 (2002) 311-316.

[22] N. Kim, S. Kee, S. H. Lee, B. H. Lee, Y. H. Kahng, Y. R. Jo, B. J. Kim, K. Lee, Highly conductive PEDOT:PSS nanofibrils induced by solution-processed crystallization, Adv. Mater. 26 (2014) 2268-2272.

[23] O. Bubnova, Z. U. Khan, A. Malti, S. Braun, M. Fahlman, M. Berggren, X. Crispin, Optimization of the thermoelectric figure of merit in the conducting polymer poly(3,4-ethylenedioxythiophene), *Nat. Mater.* 10 (2011) 429-433.

[24] N. Massonnet, A. Carella, O. Jaudouin, P. Rannou, G. Laval, C. Celle, J.-P. Simonato, Improvement of the Seebeck coefficient of PEDOT:PSS by chemical reduction combined with a novel method for its transfer using free-standing thin films, J. Mater. Chem. C 2 (2014) 1278-1283.

[25] Y. Du, K. F. Cai, S. Chen, P. Cizek, T. Lin, Facile preparation and thermoelectric properties of $Bi_2Te_3$ based alloy nanosheet/PEDOT:PSS composite films, ACS Appl. Mater. Interfaces 6 (2014) 5735-5743.

[26] B. Zhang, J. Sun, H. E. Katz, F. Fang, R. L. Opila, Promising thermoelectric properties of commercial PEDOT:PSS materials and their $Bi_2Te_3$ powder composites, ACS Appl. Mater. Interfaces 2 (2010) 3170-3178.

[27] D. Ni, H. Song, Y. Chen, K. Cai, Significantly enhanced thermoelectric performance of flexible PEDOT nanowire film *via* coating Te nanostructures, *J. Materiomics* (2019) doi.org/10.1016/j.jmat.2019.07.001.

[28] K. C. See, J. P. Feser, C. E. Chen, A. Majumdar, J. J. Urban, R. A. Segalman, Water-processable polymer-nanocrystal hybrids for thermoelectrics, Nano Lett. 10 (2010) 4664-4667.

[29] L. Wang, Z. Zhang, Y. Liu, B. Wang, L. Fang, J. Qiu, K. Zhang, S. Wang, Exceptional thermoelectric properties of flexible organic−inorganic hybrids with monodispersed and periodic nanophase, Nature Commun. 9 (2018) 3817.

[30] G. Goo, G. Anoop, S. Unithrattil, W. S. Kim, H. J. Lee, H. B. Kim, M. H. Jung, J. Park, H. C. Ko, J. Y. Jo, Proton- irradiation effects on the thermoelectric properties of flexible $Bi_2Te_3$/PEDOT:PSS composite films, Adv. Electron. Mater. 5 (2019) 1800786.

[31] Y. Lu, Y. Qiu, Q. Jiang, K. Cai, Y. Du, H. Song, M. Gao, C. Huang, J. He, D. Hu, Preparation and characterization of Te/Poly(3,4-ethylenedioxythiophene):Poly(styrenesulfonate)/$Cu_7Te_4$ ternary composite films for flexible thermoelectric power generator, ACS Appl. Mater. Interfaces 10 (2018) 42310-42319.

[32] Q. Meng, Q. Jiang, K. Cai, L. Chen, Preparation and thermoelectric properties of PEDOT:PSS coated Te nanorod/PEDOT:PSS composite films, Org. Electron. 64 (2019) 79-85.

[33] H. Ju, J. Kim, Chemically exfoliated SnSe nanosheets and their SnSe/Poly(3,4-ethylenedioxythiophene):Poly(styrenesulfonate) composite films for polymer based thermoelectric applications, ACS Nano 10 (2016) 5730-5739.

[34] D. Zhu, W. Huang, M. Song, M. Tu, Effects of annealing temperature on the electrical conductivity and mechanical property of Cu-Te alloys, J. Wuhan Uni. Tech.-Mater. Sci. Ed. 22 (2007) 88-90.

[35] J. H. We, S. J. Kim, B. J. Cho, Hybrid composite of screen-printed inorganic thermoelectric film and organic conducting polymer for flexible thermoelectric power generator, Energy 73 (2014) 506-512.

[36] M. Bharti, A. Singh, G. Saini, S. Saha, A. Bohra, Y. Kaneko, A. K. Debnath, K. P. Muthe, K. Marumoto, D. K. Aswal, S. C. Gadkari, Boosting thermoelectric power factor of free-standing

Poly(3,4ethylenedioxythiophene):polystyrenesulphonate films by incorporation of bismuth antimony telluride nanostructures, J. Power Sour. 435 (2019) 226758.

[37] S. Cao, Z. Y. Huang, F. Q. Zu, J. Xu, L. Yang, Z. G. Chen, Enhanced thermoelectric properties of Ag-modified $Bi_{0.5}Sb_{1.5}Te_3$ composites by a facile electroless plating method, ACS Appl. Mater. Interfaces 9 (2017) 36478-36482.

[38] Z. Huang, X. Dai, Y. Yu, C. Zhou, F. Zu, Enhanced thermoelectric properties of *p*-type $Bi_{0.5}Sb_{1.5}Te_3$ bulk alloys by electroless plating with Cu and annealing, Scr. Mater. 118 (2016) 19-23.

[39] Q. Zhang, Y. Sun, W. Xu, D. Zhu, Organic thermoelectric materials: emerging green energy materials converting heat to electricity directly and efficiently, Adv. Mater. 26 (2014) 6829-6851.

[40] K. E. Aasmundtveit, E. J. Samuelsen, L. A. A. Pettersson, O. Inganäs, T. Johansson, R. Feidenhans'l, Structure of thin films of poly(3,4-ethylenedioxythiophene), Synth. Metals 101 (1999) 561-564.

[41] R. Kroon, D. A. Mengistie, D. Kiefer, J. Hynynen, J. D. Ryan, L. Yu, C. Müller, Thermoelectric plastics: from design to synthesis, processing and structure–property relationships, Chem. Soc. Rev. 45 (2016) 6147-6164.

[42] O. Bubnova, X. Crispin, Towards polymer-based organic thermoelectric generators, Energy Environ. Sci. 5 (2012) 9345-9362.

[43] S. Garreau, G. Louarn, J. P. Buisson, G. Froyer, S. Lefrant, In-situ spectroelectrochemical raman studies of poly(3,4-ethylenedioxythiophene) (PEDT), Macromolecules 32 (1999) 6807-6812.

[44] M. He, J. Ge, Z. Lin, X. Feng, X. Wang, H. Lu, Y. Yang, F. Qiu, Thermopower enhancement in conducting polymer nanocomposites via carrier energy scattering at the organic–inorganic semiconductor interface, Energy Environ. Sci. 5 (2012) 8351.

[45] Z. Liang, M. J. Boland, K. Butrouna, D. R. Strachan, K. R. Graham, Increased power factors of organic–inorganic nanocomposite thermoelectric materials and the role of energy filtering, J. Mater. Chem. A 5 (2017) 15891-15900.

[46] J. Choi, J. Y. Lee, S.-S. Lee, C. R. Park, H. Kim, High-performance thermoelectric paper based on double carrier-filtering processes at nanowire heterojunctions, Adv. Energy Mater. 6 (2016) 1502181.

[47] C. Gayner, Y. Amouyal, Energy filtering of charge carriers: current trends, challenges, and prospects for thermoelectric materials, Adv. Funct. Mater. (2019) 1901789.

[48] J. Y. Lim, S. Cho, H. Kim, Y. Seo, Optimum thermoelectric performance of bismuth–antimony–telluride alloy/PEDOT:PSS nanocomposites prepared by an innovative redox process, ACS Appl. Energy Mater. (2019) 8219-8228.

[49] E. J. Bae, Y. H. Kang, K. S. Jang, C. Lee, S. Y. Cho, Solution synthesis of telluride-based nano-barbell structures coated with PEDOT:PSS for spray-printed thermoelectric generators, Nanoscale 8 (2016) 10885-10890.

[50] D. Bao, J. Chen, Y. Yu, W. Liu, L. Huang, G. Han, J. Tang, D. Zhou, L. Yang, Z.-G. Chen, Texture-dependent thermoelectric properties of nano-structured $Bi_2Te_3$, Chem. Eng. J. 388 (2020) 124295.

[51] C. Li, F. Jiang, C. Liu, W. Wang, X. Li, T. Wang, J. Xu, A simple thermoelectric device based on inorganic/organic composite thin film for energy harvesting, Chem. Eng. J. 320 (2017) 201-210.

[52] Y. Wang, W.-D. Liu, X.-L. Shi, M. Hong, L.-J. Wang, M. Li, H. Wang, J. Zou, Z.-G. Chen, Enhanced thermoelectric properties of nanostructured *n*-type $Bi_2Te_3$ by suppressing Te vacancy through non-equilibrium fast reaction, Chem. Eng. J. (2019) 123513.

[53] W.-D. Liu, L. Yang, Z.-G. Chen, J. Zou, Promising and eco-friendly $Cu_2X$-based thermoelectric materials: progress and applications, Adv. Mater. 32 (2020) 1905703.

[54] X.-L. Shi, X. Tao, J. Zou, Z.-G. Chen, High-performance thermoelectric SnSe: aqueous synthesis, innovations, and challenges, Adv. Sci. (2020) 1902923.

*Declaration of Interest Statement

**Declaration of interests**

☒ The authors declare that they have no known competing financial interests or personal relationships that could have appeared to influence the work reported in this paper.

☐The authors declare the following financial interests/personal relationships which may be considered as potential competing interests: